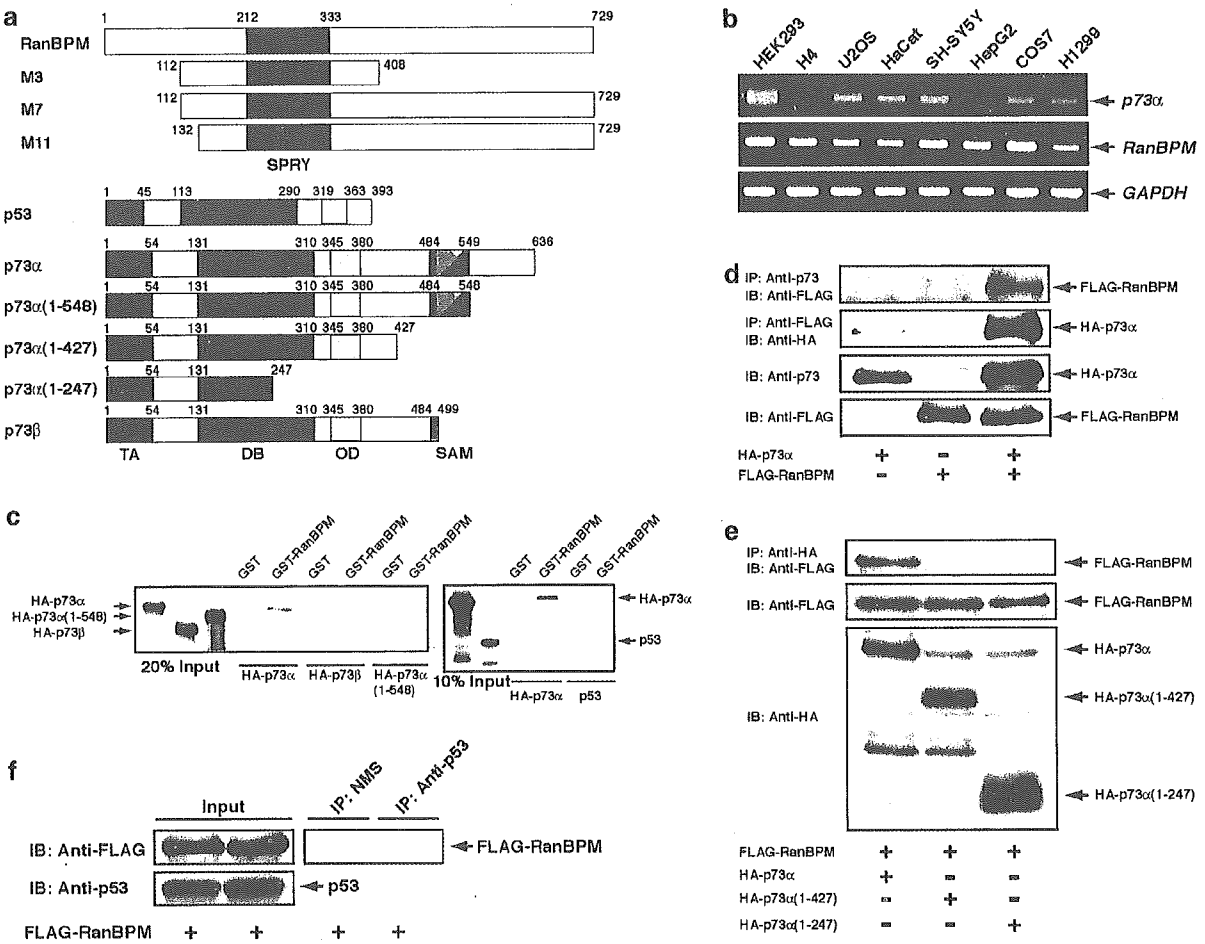

Figure 1 Identification of RanBPM as a binding partner of p73. (**a**) The three overlapping RanBPM clones (M3, M7 and M11) isolated from the yeast two-hybrid screening along with the full-length RanBPM are shown. The putative SPRY domain (amino-acid residues 212–333) is indicated. Structures of p73 and p53 are also shown. TA, transactivation domain; DB, DNA-binding domain; OD, oligomerization domain; SAM, sterile α motif domain. Amino-acid numbering was relative to first methionine, which represents position +1. (**b**) Expression of *RanBPM* and *p73*. Total RNA prepared from the indicated cell lines were incubated with SuperScript II reverse transcriptase (Invitrogen, Carlsbad, CA, USA), and generated cDNAs were amplified by PCR in the presence of primers specific for *p73* (top panel), *RanBPM* (middle panel) or *GAPDH* (bottom panel). (**c**) GST pull-down assay. *In vitro* translated ^{35}S-labeled p73α, p73β, p73α (1–548) or p53 was incubated with bacterially expressed GST or GST-RanBPM(112–408) for 2 h at 4°C. Bound complexes were recovered on the glutathione–sepharose beads (Amersham Pharmacia Biotech, Piscataway, NJ, USA), washed extensively with the binding buffer (50 mM Tris–HCl, pH 7.5, 150 mM NaCl, 0.1% Nonidet P-40, 1 mM EDTA, and 1 mM phenylmethylsulfonyl fluoride), and then boiled in SDS sample buffer. Bound proteins were resolved by 10% SDS–polyacrylamide gel, and analysed by autoradiography. The input of the radio-labeled proteins used in the binding reaction is also shown. (**d**) p73α interacts with RanBPM in mammalian cultured cells. COS7 cells transfected with the indicated expression plasmids were lysed in 25 mM Tris–HCl, pH 8.0, 137 mM NaCl, 1% Triton X-100 and 1 mM phenylmethylsulfonyl fluoride. Whole-cell lysates were immunoprecipitated with anti-p73 antibody (Ab-4, NeoMarkers, Fremont, CA, USA) or anti-FLAG (M2, Sigma, St Louis, MO, USA), and subjected to immunoblotting with anti-FLAG (first panel) or with anti-HA (12CA5, Roche Molecular Biochemicals, Indianapolis, IN, USA) antibody (second panel), respectively. Separate aliquots of the lysates were immunoblotted with anti-p73 (third panel) or anti-FLAG antibody (fourth panel) to confirm the expression of FLAG-RanBPM or HA-p73α, respectively. (**e**) COOH-terminal region of p73α is required for the interaction with RanBPM. COS7 cells were co-transfected with the indicated combinations of the expression plasmids, and whole-cell lysates were immunoprecipitated with anti-HA antibody, followed by immunoblotting with anti-FLAG antibody (top panel). Cell lysates were immunoblotted as a control for FLAG-RanBPM (middle panel), HA-p73α and HA-p73α derivatives (bottom panel) in the input lysate. (**f**) p53 does not bind to RanBPM. Cell lysates prepared from COS7 cells transfected with FLAG-RanBPM were immunoprecipitated with the normal mouse serum (NMS, Jackson ImmunoResearch Laboratories, West Grove, PA, USA) or anti-p53 antibodies (DO-1 plus PAb1801, Oncogene Research Products, Cambridge, MA, USA). Immunoprecipitates were analysed by immunoblotting with anti-FLAG antibody (right panel). Left panels show the Western blotting with anti-FLAG, or anti-p53 antibody to monitor the expression level of FLAG-RanBPM or the endogenous p53, respectively

unlikely that RanBPM is involved in this process (Nishitani *et al*., 2001). Alternatively, Nakamura *et al*. (1998) reported that RanBPM might be involved in reorganization of the microtubule network; however, the precise function of RanBPM remains unknown. Consistent with the previous observations (Rao *et al*., 2002), *RanBPM* was expressed in various cell lines (Figure 1b). To confirm the interaction between RanBPM and p73, we performed GST pull-down assays using a GST fusion protein containing RanBPM

(112–408) and *in vitro* translated ^{35}S-labeled p73α, p73β, p73α(1–548) or p53. GST alone was employed as a negative control. As shown in Figure 1c, radio-labeled p73α was pulled down by GST-RanBPM(112–408) but not by GST alone. However, p73β and p73α(1–548), which lack the extreme COOH-terminal portion of p73α, were no longer able to interact with GST-RanBPM(112–408). In addition, p53 failed to bind to GST-RanBPM(112–408). In good agreement with the yeast two-hybrid results, these observations suggest that the extreme COOH-terminal portion of p73α is responsible for the physical interaction with RanBPM. Next, we performed co-immunoprecipitation experiments to confirm their interaction in cells. To this end, cell lysates prepared from COS7 cells co-transfected with HA-tagged p73α and FLAG-tagged full-length RanBPM were immunoprecipitated with anti-p73 or anti-FLAG antibody, followed by immunoblotting with anti-FLAG or anti-HA antibody, respectively. As shown in Figure 1d, HA-p73α co-immunoprecipitated with FLAG-RanBPM. Under our experimental conditions, HA-p73α(1–427) and HA-p73α(1–247) did not co-immunoprecipitate with FLAG-RanBPM (Figure 1e). In contrast to full-length p73α, the anti-p53 immunoprecipitates did not contain FLAG-RanBPM (Figure 1f). Taken together, our results suggest that RanBPM has an ability to interact with p73α but not with p53 in mammalian cultured cells.

Previous immunostaining studies have shown that p73α is exclusively localized in cell nucleus (Jost *et al.*, 1997), while RanBPM could distribute to the cell nucleus, perinuclear region and cytoplasm (Nishitani *et al.*, 2001; Umeda *et al.*, 2003). To examine the subcellular localization of RanBPM in the presence or absence of p73α, COS7 cells were transfected with the indicated expression plasmids, and the indirect immunofluorescent staining was performed. As shown in Figure 2a and b, FLAG-RanBPM and HA-p73α were detected largely in the cytoplasm and cell nucleus, respectively. Of note, when FALG-RanBPM was co-expressed with HA-p73α, a fraction of FLAG-RanBPM translocated into cell nucleus, and co-localized with nuclear HA-p73α (Figure 2c–e). To confirm this issue, transfected COS7 cells were fractionated into nuclear and cytoplasmic fractions, and their subcellular localizations were analysed by immunoblotting. The purity of the nuclear and cytoplasmic fractions was examined by immunoblotting with anti-Lamin B and anti-α-tubulin antibody, respectively. Consistent with the indirect immunofluorescent staining, co-expression of FLAG-RanBPM with HA-p73α resulted in a significant nuclear accumulation of FLAG-RanBPM, whereas FLAG-RanBPM alone was detected in the cytoplasmic fraction (Figure 2f). In addition, the amounts of nuclear HA-p73α seemed to be increased in the presence of FLAG-RanBPM. It is thus likely that RanBPM interacts with p73α in cell nucleus, and could affect the stability of p73α.

To test whether RanBPM could affect the stability of p73α, COS7 cells were co-transfected with the constant amount of HA-p73α together with or without the

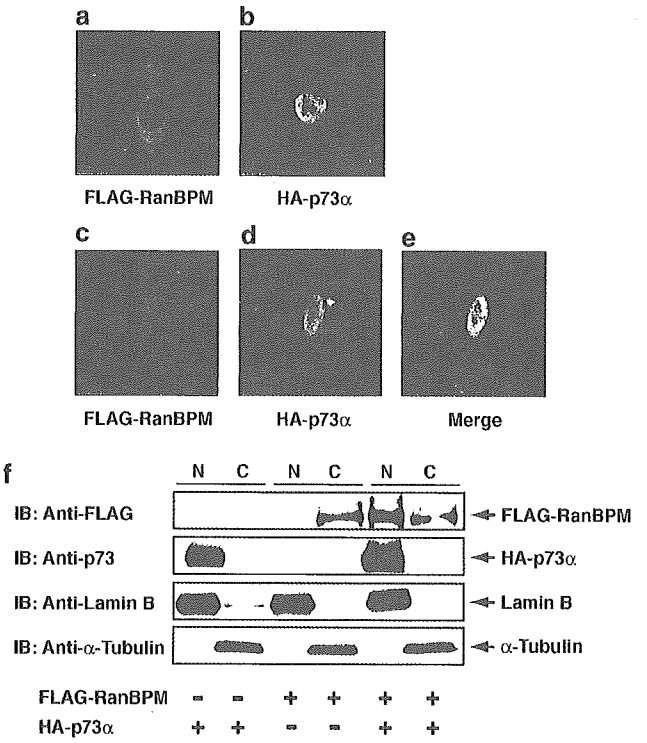

Figure 2 Subcellular distribution of RanBPM in the presence of p73. (**a–e**) Nuclear co-localization of p73α and RanBPM by immunofluorescence. COS7 cells were transfected with FLAG-RanBPM (**a**), HA-p73α (**b**) or FLAG-RanBPM and HA-p73α (**c–e**). At 48 h after transfection, cells were fixed in 20% methanol and incubated with anti-FLAG (red) and anti-HA antibody (green) (Medical and Biological Laboratories, Nagoya, Japan), followed by the incubation with the rhodamine- and FITC-conjugated secondary antibodies (Jackson ImmunoResearch Laboratories), respectively. Cells were then examined under a confocal scanning laser microscope. The merged images of the two signals are displayed in yellow (**e**). (**f**) Fractionation of COS7 cell extracts. COS7 cells were transfected with the indicated expression plasmids. At 48 h after transfection, cells were fractionated into nuclear (N) and cytoplasmic (C) fractions, and then analysed directly by immunoblotting with anti-FLAG (first panel) or anti-p73 antibody (second panel). The nuclear or cytoplasmic fraction was confirmed by immunoblotting with anti-Lamin B (Ab-1, Oncogene Research Products) (third panel) or anti-α-tubulin antibody (DM1A, Cell Signaling Technology, Beverly, MA, USA) (fourth panel), respectively

increasing amounts of FLAG-RanBPM. As shown in Figure 3a, the amount of HA-p73α was markedly increased in the presence of FLAG-RanBPM in a dose-dependent manner, whereas the expression level of p73α mRNA remained unchanged. On the other hand, FLAG-RanBPM had no significant effect on the levels of exogenous p53 (Figure 3b). Similar results were also obtained in p53-deficient H1299 cells (data not shown). We next sought to determine the half-life of p73α in the presence of RanBPM. For this purpose, COS7 cells were transfected with HA-p73α together with or without FLAG-RanBPM. At 24 h after transfection, cells were treated with cycloheximide. At the indicated time periods, cell lysates were analysed for HA-p73α by immunoblotting. In accordance with the previous reports (Lee and La Thangue, 1999; Ohtsuka *et al.*,

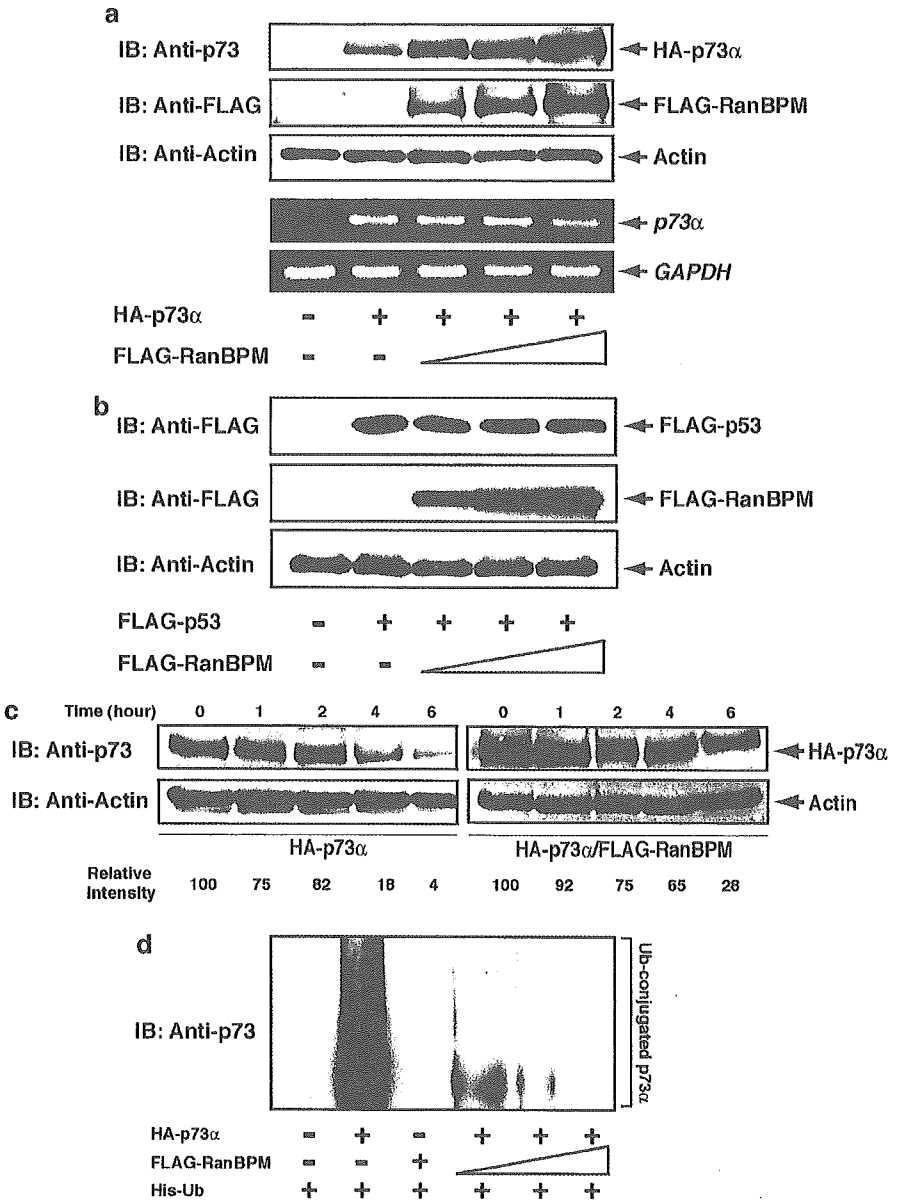

Figure 3 RanBPM increases the stability of p73 but not of p53. (**a**) RanBPM increases the amounts of p73α. COS7 cells were co-transfected with the constant amount of HA-p73α (0.5 μg) together with or without the increasing amounts of FLAG-RanBPM (0.5, 1.0 and 1.5 μg). The total amount of plasmid DNA was kept constant (2 μg) with pcDNA3. At 48 h after transfection, cell lysates or total RNA were prepared, and subjected to immunoblotting with the indicated antibodies (upper panels) or RT–PCR analysis (lower panels). Immunoblotting for actin (20–33, Sigma Chemical Co.) serves as a loading control. (**b**) RanBPM does not affect the amounts of p53. COS7 cells were co-transfected with the indicated combinations of the expression plasmids, and were processed for immunoblotting as described above. (**c**) RanBPM increases the half-life of p73α. COS7 cells were transfected with HA-p73α alone (0.5 μg) (left panels) or together with FLAG-RanBPM (1.5 μg) (right panels). At 24 h post-transfection, cells were treated with cycloheximide (100 μg/ml) and harvested at the indicated time periods. Cell lysates were used for immunoblotting with the indicated antibodies. The intensity of the bands was quantified by using densitometry. (**d**) RanBPM inhibits the ubiquitination of p73α. COS7 cells were co-transfected with the constant amount of HA-p73α (0.5 μg) and His-tagged ubiquitin (Ub) (0.5 μg), together with or without the increasing amounts of FLAG-RanBPM (0.5, 1.0 and 1.5 μg). At 24 h post-transfection, cells were treated with 20 μM MG-132 for 6 h before being harvested. His-tagged ubiquitin-containing protein complexes were pulled down with Ni^{2+}-agarose beads (QIAGEN, Valencia, CA, USA), and subsequently resolved by 10% SDS–polyacrylamide gel electrophoresis, followed by immunoblotting with anti-p73 antibody

2003), ectopically expressed p73α had a half-life of less than 4 h, whereas the degradation rate of HA-p73α was slower in FLAG-RanBPM-expressing cells (Figure 3c). Thus, it is likely that the RanBPM-dependent stabilization of p73α is attributed to the clear increase in the half-life of p73α.

As described (Balint *et al*., 1999), the stability of p73 is regulated at least in part through the ubiquitin–proteasome pathway. These observations prompted us to determine whether RanBPM could prevent the ubiquitination of p73. COS7 cells were transfected with HA-p73α- and His-tagged ubiquitin, or in combination

with the increasing amounts of FLAG-RanBPM. At 24 h after transfection, cells were treated with MG-132 for 6 h. His-ubiquitinated proteins were purified by Ni^{2+}-agarose beads, and then analysed by immunoblotting with the anti-p73 antibody. As shown in Figure 3d, the slower migrating ubiquitinated forms of p73α were detectable in the absence of FLAG-RanBPM. Intriguingly, the ubiquitination levels of p73α were significantly reduced in cells expressing FLAG-RanBPM, suggesting that RanBPM stabilizes p73α by inhibiting its ubiquitination.

To determine whether RanBPM could affect the transcriptional activity of p73α, H1299 cells were transiently transfected with a constant amount of the expression plasmid for HA-p73α, together with the p53/p73-responsive *p21^{WAF1}* or *MDM2* luciferase reporter constructs in the presence or absence of increasing amounts of the FLAG-RanBPM expression plasmid. As shown in Figure 4a, expression of FLAG-RanBPM enhanced the ability of p73α to transactivate the *p21^{WAF1}* and *MDM2* promoters in a dose-dependent manner. To extend the functional significance of their interaction, we examined the possible effect of RanBPM on the p73α-mediated apoptosis. H1299 cells were transfected with HA-p73α, FLAG-RanBPM, or HA-p73α and FLAG-RanBPM. The β-galactosidase was used as a marker to visualize the transfected cells. At 48 h post transfection, the number of β-galactosidase-positive cells was scored. As shown in Figure 4b, the number of β-galactosidase-positive cells expressing FLAG-RanBPM was similar to that detected in the empty plasmid-transfected cells. Consistent with the previous report (Watanabe *et al.*, 2002), expression of HA-p73α resulted in a clear decrease in the number of β-galactosidase-positive cells. Of note, co-expression of HA-p73α with FLAG-RanBPM significantly reduced the number of β-galactosidase-positive cells as compared with that observed in cells expressing HA-p73α alone. In addition, we performed a colony formation assay. H1299 cells were transfected with HA-p73α, FLAG-RanBPM or HA-p73α plus FLAG-RanBPM, and the transfected cells were selected in the presence of G418. After 2 weeks of selection, drug-resistant colonies were fixed and stained with Giemsa's solution. In accordance with the β-galactosidase assay, FLAG-RanBPM expression did not affect the colony formation as compared with the empty plasmid-transfected control, whereas co-expression of HA-p73α with FLAG-RanBPM reduced the colony formation even more efficiently than HA-p73α alone (Figure 4c). Considering that p73α efficiently induced apoptosis in H1299 cells (Di Como *et al.*, 1999; Zeng *et al.*, 1999), these results suggest that RanBPM increases the proapoptotic activity of p73α. To further confirm this issue, H1299 cells were transiently transfected with a constant amount of the GFP expression plasmid along with the indicated combinations of the expression plasmids. At 48 h after transfection, transfected cells were identified by fluorescence microscopy for the appearance of green fluorescence, and the number of GFP-positive cells with condensed and fragmented nuclei was counted. As shown in Figure 4d, co-expression of HA-p73α with FLAG-RanBPM increased the number of apoptotic cells as compared with that resulting from expression of HA-p73α alone. Taken together, our present results strongly suggest that RanBPM-mediated stabilization of p73α is critical for its effects on transcriptional activation as well as apoptosis.

Recently, it has been shown that a variety of cellular proteins could interact with RanBPM, including MET, androgen receptor, HIPK2, USP11, Twa1, calbindin D28K and p75^{NTR}, suggesting that RanBPM is involved in diverse biological processes (Ideguchi *et al.*, 2002; Rao *et al.*, 2002; Wang D *et al.*, 2002; Wang Y *et al.*, 2002; Bai *et al.*, 2003; Lutz *et al.*, 2003; Umeda *et al.*, 2003). In the present study, we demonstrated that RanBPM increased the stability of p73α by reducing its ubiquitination levels. An important question raised by our results is how RanBPM stabilize p73α. Intriguingly, Ideguchi *et al.* (2002) described that RanBPM is associated with the deubiquitination enzyme USP11, which belongs to the ubiquitin hydrolase family. Considering that p53 is stabilized by direct deubiquitination by the deubiquitination enzyme HAUSP (Li *et al.*, 2002), it is likely that RanBPM could bind to USP11 and promote deubiquitination of p73α by recruiting USP11 to p73α; however, further studies will be required to determine this issue.

Alternatively, Lee and La Thangue (1999) found that p73β is much more stable than p73α, suggesting that the unique COOH-terminal portion of p73α might be critical for degradation by the ubiquitin–proteasome system. According to our present results, RanBPM bound to p73α through its extreme COOH-terminal region, whereas it failed to interact with p73β. Thus, it is plausible that RanBPM might increase the steady-state levels of p73α by masking p73α COOH-terminal lysine residues, which could be the sites for ubiquitin ligation, and/or disrupting the interaction of p73α with unknown proteins required for ubiquitination-mediated proteolysis. These possibilities are currently under investigation. Elucidation of the detailed molecular mechanism underlying the RanBPM-dependent stabilization of p73α would be necessary for better understanding of p73 turnover.

Another finding of the present study is that, under our experimental conditions, cytoplasmic RanBPM became nuclear in the presence of p73α overexpression. Given that RanBPM is localized in both the cytoplasm and nucleus (Nakamura *et al.*, 1998; Nishitani *et al.*, 2001), it is probable that p73α might have an ability to promote nuclear translocation of RanBPM through the physical interaction between them. As described previously, wild-type p53 is predominantly localized in the cytoplasm of many neuroblastoma cells (Moll *et al.*, 1996). The abnormal cytoplasmic distribution of p53 might be attributed at least in part to the interaction with Parc, which acts as a cytoplasmic anchor protein for p53 (Nikolaev *et al.*, 2003). Interestingly, Goldschneider *et al.* (2004) found that enforced expression of p73α in neuroblastoma-derived SH-SY5Y cells significantly enhances the nuclear accumulation of wild-type p53 and

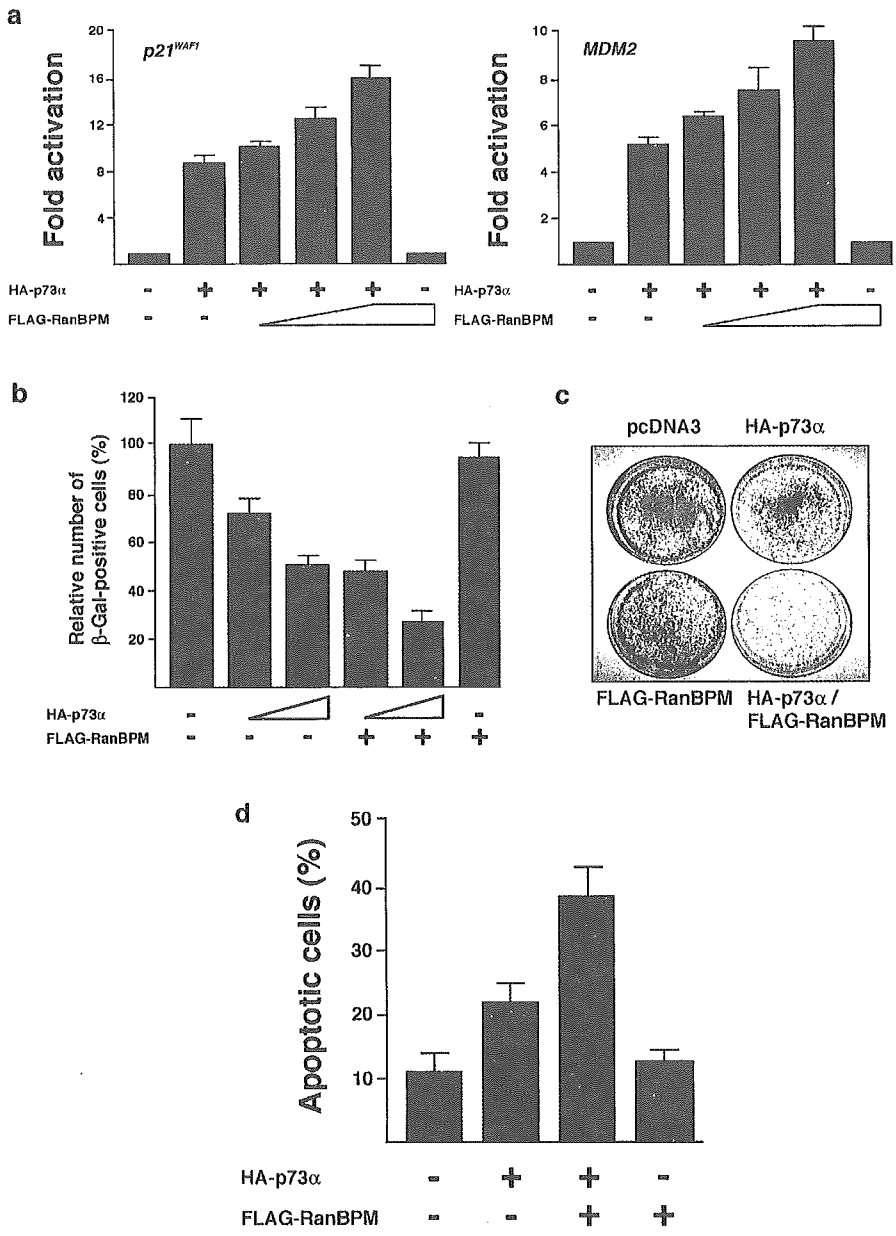

Figure 4 RanBPM enhances p73 function. (**a**) RanBPM enhances the transcriptional activity of p73α. p53-deficient H1299 cells were co-transfected with 25 ng of the expression plasmid for HA-p73α together with 100 ng of p53/p73-responsive *p21*^{WAF1} (left panel) or *MDM2* (right panel) luciferase reporter construct, and 10 ng of the *Renilla* luciferase plasmid (pRL-TK, Promega Corp., Madison, WI, USA), in the presence or absence of increasing amounts of the FLAG-RanBPM expression plasmid (25, 50, or 100 ng). At 48 h after transfection, cells were lysed and their luciferase activities were measured. Firefly luminescence signal was normalized based on the *Renilla* luminescence signal. (**b**) RanBPM stimulates the p73α-mediated growth suppression. H1299 cells were co-transfected with the indicated combinations of the expression plasmid together with the constant amount of the expression plasmid for β-galactosidase (125 ng) (pCH110, Amersham Pharmacia Biotech). At 48 h after transfection, transfected cells were identified by staining with 5-bromo-4-chloro-3-indolyl-β-D-galactopyranoside (X-gal). The relative percentage of β-gal-positive cells represents the ratio of the number of β-gal-positive cells to that of those transfected with pcDNA3 alone. (**c**) Colony formation assay. H1299 cells were transfected with HA-p73α (200 ng), FLAG-RanBPM (750 ng) or HA-p73α (200 ng) plus FLAG-RanBPM (750 ng). Total amount of plasmid DNA was kept constant (1 μg) with pcDNA3, and pcDNA3 alone was used as a negative control. At 2 days after transfection, cells were selected with G418 (400 μg/ml) for 2 weeks. G418-resistant colonies were fixed in methanol, and stained with Giemsa's solution. Representative dishes of three independent experiments are shown. (**d**) RanBPM enhances the p73α-mediated apoptosis. H1299 cells transfected with 0.2 μg of the GFP expression plasmid and 0.5 μg of the HA-p73α expression plasmid together with or without 1.5 μg of the FLAG-RanBPM expression plasmid. At 48 h after transfection, transfected cells were identified by the presence of green fluorescence. Cell nucleus was stained with DAPI to reveal nuclear condensation and fragmentation. The number of GFP-positive cells with apoptotic nuclei was scored

restores its function, indicating that p73α displaces p53 from the cytoplasmic complex containing Parc. It is thus likely that p73α could modulate cellular proteins/pathways that specifically regulate nuclear import and export of RanBPM. Since RanBPM is associated with a variety of nuclear proteins, p73α might play a critical role in regulating nuclear function of RanBPM.

Acknowledgements
We are grateful to Dr S Sakiyama for helpful discussion. This work was supported in part by a Grant-in-Aid from the Ministry of Health and Welfare for a New 10-Year Strategy for Cancer Control, a Grant-in-Aid for Scientific Research on Priority Areas, a Grant-in-Aid for Scientific Research (B) from the Ministry of Education, Science, Sports and Culture, Japan, and a found from the Hisamitsu Pharmaceutical Company.

References

Agami R, Blandino G, Oren M and Shaul Y. (1999). *Nature*, **399,** 809–813.
Bai D, Chen H and Huang BR. (2003). *Biochem. Biophys. Res. Commun.*, **309,** 552–557.
Balint E, Bates S and Vousden KH. (1999). *Oncogene*, **18,** 3923–3929.
Carrano AC, Eytan E, Hershko A and Pagano M. (1999). *Nat. Cell Biol.*, **1,** 193–199.
Di Como CJ, Gaiddon C and Prives C. (1999). *Mol. Cell. Biol.*, **19,** 1438–1449.
Ganoth D, Bornstein G, Ko TK, Larsen B, Tyers M, Pagano M and Hershko A. (2001). *Nat. Cell Biol.*, **3,** 321–324.
Goldschneider D, Blanc E, Raguenez G, Barrois M, Legrand A, Le Roux G, Haddada H, Bebard J and Douc-Rasy S. (2004). *J. Cell Sci.*, **117,** 293–301.
Gong J, Costanzo A, Yang H-Q, Melino G, Kaelin WG, Levrero M and Wang JYJ. (1999). *Nature*, **399,** 806–809.
Ideguchi H, Ueda A, Tanaka M, Yang J, Tsuji T, Ohno S, Hagiwara E, Aoki A and Ishigatsubo Y. (2002). *Biochem. J.*, **367,** 87–95.
Jost C, Marin M and Kaelin WG. (1997). *Nature*, **389,** 191–194.
Kaghad M, Bonnet H, Yang A, Creancier L, Biscan JC, Valent A, Minty A, Chalon P, Lelias JM, Dumont X, Ferrara P, McKeon F and Caput D. (1997). *Cell*, **90,** 809–819.
Lee C-W and La Thangue NB. (1999). *Oncogene*, **18,** 4171–4181.
Li M, Chen D, Shiloh A, Luo J, Nikolaev AY, Qin J and Gu W. (2002). *Nature*, **416,** 648–653.
Lutz W, Frank EM, Craig TA, Thompson R, Venters RA, Kojetin D, Cavanagh J and Kumar R. (2003). *Biochem. Biophys. Res. Commun.*, **303,** 1186–1192.
Melino G, De Laurenzi V and Vousden KH. (2002). *Nat. Rev. Cancer*, **2,** 605–615.
Moll UM, Ostermeyer AG, Haladay R, Winkfield B, Frazier M and Zambetti G. (1996). *Mol. Cell. Biol.*, **16,** 1126–1137.
Nakagawa T, Takahashi M, Ozaki T, Watanabe K, Todo S, Mizuguchi H, Hayakawa T and Nakagawara A. (2002). *Mol. Cell. Biol.*, **22,** 2575–2585.
Nakamura M, Masuda H, Horii J, Kuma K, Yokoyama N, Ohba T, Nishitani H, Miyata T, Tanaka M and Nishimoto T. (1998). *J. Cell Biol.*, **143,** 1041–1052.
Nikolaev AY, Li M, Puskas N, Qin J and Gu W. (2003). *Cell*, **112,** 29–40.
Nishitani H, Hirose E, Uchimura Y, Nakamura N, Umeda M, Nishii K, Mori N and Nishimoto T. (2001). *Gene*, **272,** 25–33.
Ohtsuka T, Ryu H, Minamishima YA, Ryo A and Lee SW. (2003). *Oncogene*, **22,** 1678–1687.
Ozaki T, Watanabe K, Nakagawa T, Miyazaki K, Takahashi M and Nakagawara A. (2003). *Oncogene*, **22,** 3231–3242.
Ponting C, Schultz J and Bork P. (1997). *Trends Biochem. Sci.*, **22,** 193–194.
Pozniak CD, Radinovic S, Yang A, McKeon F, Kaplan DR and Miller FD. (2000). *Science*, **289,** 304–306.
Rao MA, Cheng H, Quayle AN, Nishitani H, Nelson CC and Rennie PS. (2002). *J. Biol. Chem.*, **277,** 48020–48027.
Ren J, Datta R, Shioya H, Li Y, Oki E, Biedermann V, Bharti A and Kufe D. (2002). *J. Biol. Chem.*, **277,** 33758–33765.
Stiewe T, Zimmermann S, Frilling A, Esche H and Putzer BM. (2002). *Cancer Res.*, **62,** 3598–3602.
Umeda M, Nishitani H and Nishimoto T. (2003). *Gene*, **303,** 47–54.
Wang D, Li Z, Messing EM and Wu G. (2002). *J. Biol. Chem.*, **277,** 36216–36222.
Wang Y, Schneider M, Li X, Duttenhofer I, Debatin K-M and Hug H. (2002). *Biochem. Biophys. Res. Commun.*, **297,** 148–153.
Watanabe K, Ozaki T, Nakagawa T, Miyazaki K, Takahashi M, Hosoda M, Hayashi S, Todo S and Nakagawara A. (2002). *J. Biol. Chem.*, **277,** 15113–15123.
Yuan Z-M, Shioya H, Ishiko T, Sun X, Gu J, Huang YY, Lu H, Kharbanda S, Weichselbaum R and Kufe D. (1999). *Nature*, **399,** 814–817.
Zeng X, Chen L, Jost CA, Maya R, Keller D, Wang X, Kaelin WG, Oren M, Chen J and Lu H. (1999). *Mol. Cell. Biol.*, **19,** 3257–3266.

CpG Island Methylator Phenotype Is a Strong Determinant of Poor Prognosis in Neuroblastomas

Masanobu Abe,[1,2] Miki Ohira,[3] Atsushi Kaneda,[1] Yukiko Yagi,[1] Seiichiro Yamamoto,[4] Yoshihiro Kitano,[5] Tsuyoshi Takato,[2] Akira Nakagawara,[3] and Toshikazu Ushijima[1]

[1]Carcinogenesis Division, National Cancer Center Research Institute; [2]Department of Oral and Maxillo Facial Surgery, University of Tokyo Graduate School of Medicine; [3]Biochemistry Division, Chiba Cancer Center Research Institute; [4]Information Division, Research Center for Cancer Prevention and Screening, National Cancer Center; and [5]Department of Pediatric Surgery, National Center for Child Health and Development, Tokyo, Japan

Abstract

Neuroblastoma, one of the most common pediatric solid tumors, is characterized by two extreme disease courses, spontaneous regression and life-threatening progression. Here, we conducted a genome-wide search for differences in DNA methylation that distinguish between neuroblastomas of the two types. Three CpG islands (CGI) and two groups of CGIs were found to be methylated specifically in neuroblastomas with a poor prognosis. By quantitative analysis of 140 independent cases, methylation of all the five CGI (groups) was shown to be closely associated with each other, conforming to the CpG island methylator phenotype (CIMP) concept. The presence of CIMP was sensitively detected by methylation of the *PCDHB* CGIs and associated with significantly poor survival (hazard ratio, 22.1; 95% confidence interval, 5.3-93.4; $P < 0.0001$). Almost all cases with N-*myc* amplification (37 of 38 cases) exhibited CIMP. Even in 102 cases without N-*myc* amplification, the presence of CIMP (30 cases) strongly predicted poor survival (hazard ratio, 12.4; 95% confidence interval, 2.6-58.9; $P = 0.002$). Methylation of *PCDHB* CGIs, located in their gene bodies, did not suppress gene expression or induce histone modifications. However, CIMP was significantly associated with methylation of promoter CGIs of the *RASSF1A* and *BLU* tumor suppressor genes. The results showed that neuroblastomas with CIMP have a poor prognosis and suggested induction of silencing of important genes as an underlying mechanism. (Cancer Res 2005; 65(3): 828-34)

Introduction

Epigenetic abnormalities, especially alterations in DNA methylation, are intimately involved in development of various human tumors (1). Aberrant methylation of promoter CpG islands (CGI) causes inactivation of tumor suppressor genes. Genomic instability is caused by genomic hypomethylation and is associated with hypermethylation (2, 3). Identification of epigenetic abnormalities in human cancers is expected to lead not only to discovery of novel disease mechanisms but also to development of new diagnostic markers. Therefore, we previously developed a genome-wide scanning method, methylation-sensitive representational difference analysis (MS-RDA), for detecting differences in DNA methylation (4, 5). This technique analyzes unmethylated, CpG-rich regions of the genome and has already identified genes silenced in human lung, stomach, breast, and pancreatic cancers (6–9).

Neuroblastoma derived from primitive cells of the sympathetic nervous system is one of the most common solid tumors in childhood, characterized by two extreme disease courses, spontaneous regression, and life-threatening progression (10, 11). The clinical outcome is associated with disease stage, age at diagnosis, histologic classification, N-*myc* amplification, DNA ploidy, and *TrkA* overexpression (10–12). These characteristics are therefore used to classify cases into low-, intermediate-, and high-risk groups. However, especially in the cases with intermediate risk, prediction of prognosis and therapeutic decision-making are still difficult, and development of new markers is an urgent priority. Moreover, the molecular bases underlying the two distinct clinical courses are still unknown, and their clarification is needed to allow development of novel therapeutics.

In the present study, considering the major involvement of epigenetic machinery in embryonic development (13, 14), we searched for differences in DNA methylation between neuroblastomas with a good prognosis and counterparts with a poor prognosis by MS-RDA.

Materials and Methods

Tissue Samples and Cell Lines. Tumor samples were obtained from 145 nonrecurrent cases between 1995 and 1999 and were used under approval of institutional review boards. The mean age at initial diagnosis was 27 months (range, 0-216 months). Their clinical stages were determined according to the International Neuroblastoma Staging System, and 40, 17, 20, 60, and 8 cases belonged to stages I, II, III, IV, and IVS, respectively. Normal adrenal medulla tissue was collected from a case undergoing nephrectomy for a renal cancer. Neuroblastoma cell lines were obtained from the American Type Culture Collection (Manassas, VA), the Japanese Collection of Research Bioresources (Tokyo, Japan), and the RIKEN Bio Resource Center (Tsukuba, Japan). GANB was established by A.N. and normal human bronchial epithelial cells were purchased from Cambrex (East Rutherford, NJ). High molecular weight DNA and total RNA were extracted as previously described (7). Total RNAs of brain and adrenal glands were purchased from Clontech (Palo Alto, CA).

MS-RDA and Database Search. MS-RDA was done as previously described (4, 5). Genomic DNA of primary neuroblastomas with a good prognosis (cases 92, 98, 104, 112, and 148) and neuroblastoma cell lines established from cases with a poor prognosis (CHP134, IMR32, GANB, NGP, and TGW) were digested with *Hpa*II, and then two pooled DNA samples were prepared. Although use of cell lines is highly recommended for MS-RDA (5), no cell lines were available for neuroblastomas with a good prognosis, and therefore we used the primary samples. To isolate CGIs that were hypermethylated in the latter, the cell line pool was used as the tester, and the primary tumor pool as the driver. MS-RDA in the opposite direction

Note: Supplementary data for this article are available at Cancer Research online (http://cancerres.aacrjournals.org/).

Requests for reprints: Toshikazu Ushijima, 5-1-1 Tsukiji, Chuo-ku, Tokyo 104-0045, Japan. Phone: 133-547-5240; Fax: 135-565-1753; E-mail: tushijim@ncc.go.jp.

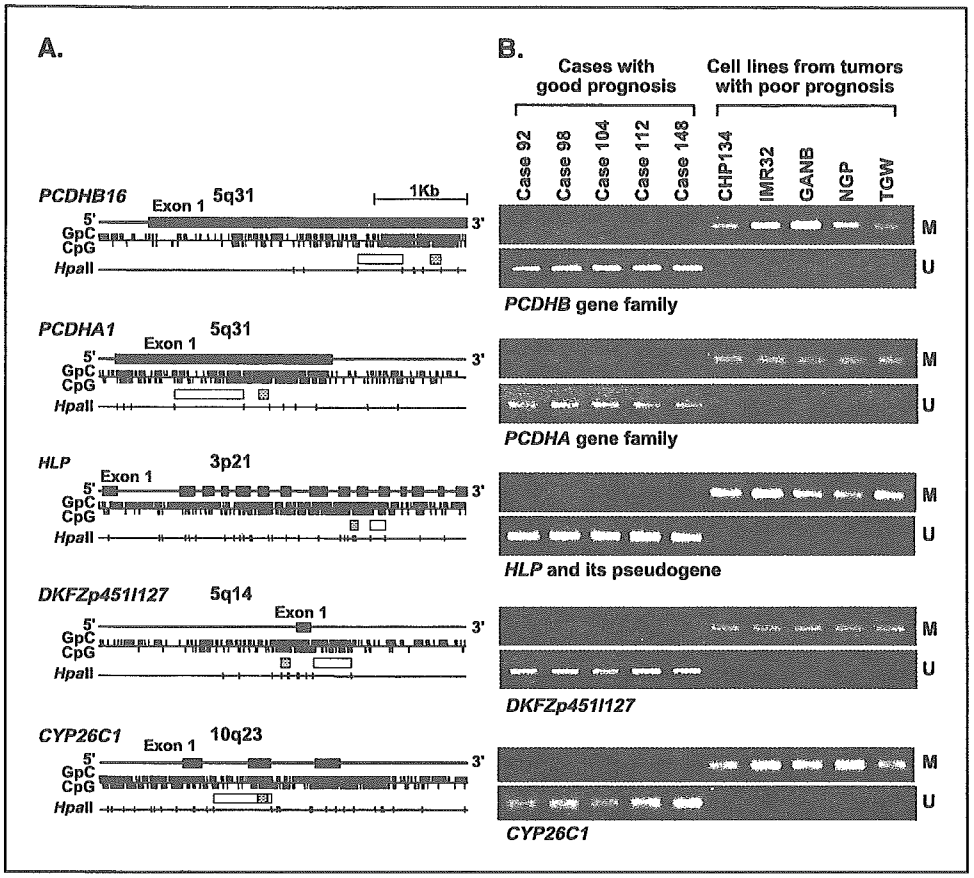

Figure 1. Five CGIs isolated by MS-RDA and their methylation statuses in the samples used for MS-RDA. *A*, genomic structures of the five CGIs. GpC, CpG, and *Hpa*II recognition sites (5′-CCGG-3′) are shown by ticks. *Closed boxes*, exons; *open boxes*, clones isolated by MS-RDA; *shaded boxes*, regions analyzed by MSP. *B*, methylation statuses analyzed by MSP. *M*, MSP using primers specific to methylated DNA; *U*, MSP using primers specific to unmethylated DNA. All the five CGIs were found to be differentially methylated between the two groups used for MS-RDA.

was also done. For each series of MS-RDA, 96 clones were analyzed for redundancy, and nonredundant clones were sequenced. Their genomic origins were examined using BLASTN software http://www.ncbi.nlm.nih.gov/BLAST/).

Sodium Bisulfite Modification and Methylation-Specific PCR. One microgram of DNA underwent sodtlbium bisulfite modification (15), and was suspended in 20 μL of TE buffer. For methylation-specific PCR (MSP), 1 μL of the solution was used for PCR with primers specific to methylated or unmethylated sequences. Using DNA from normal human bronchial epithelial and DNA methylated with *Sss*I methylase, annealing temperatures specific for methylated and unmethylated primers were determined. Quantitative MSP was done separately for methylated DNA molecules and for unmethylated DNA molecules. Standard DNA was prepared by cloning PCR products amplified by methylated and unmethylated primers into a vector, respectively. The numbers of methylated and unmethylated molecules in a test sample were determined by comparing their amplification with those of standard samples containing 10 to 10^6 molecules. The "methylation index" was calculated as the fraction of methylated molecules in the total DNA molecules (no. methylated molecules + no. unmethylated molecules). Each sample was analyzed twice, blind to clinical information, and high reproducibility was confirmed (correlation coefficient = 0.98).

The *protocadherin* β (*PCDHB*) family consists of 16 genes with single exons and three pseudogenes on 5q31, and their CGIs are located in the gene bodies. MSP primers were designed to recognize 17 of the 19 members (all except for the *PCDHB1* gene and the *PCDHB19* pseudogene). The *protocadherin* α (*PCDHA*) family consists of 15 genes and one pseudogene having unique first exons and shared exons 2 to 4 on 5q31, and their CGIs are located in exon 1. MSP primers were designed to recognize 13 of the 16 members (all except for the *PCDHAC1* and *PCDHAC2* genes and the *PCDHA14* pseudogene). The *hepatocyte growth factor-like protein* (*HLP/MSP/MST1*) gene is highly homologous to *macrophage stimulating, pseudogene 9* (*MSTP9*), and MSP primers were designed to recognize both of these. For *DKFZp451I127*, *FLJ37440*, *Zinc finger protein 297* (*ZNF297*), and *Cytochrome p450 CYP26C1* (*CYP26C1*), MSP primers were designed to recognize each of them specifically. The primers and PCR conditions are shown in Supplementary Table 1.

Semiquantitative and Quantitative Reverse Transcription-PCR. cDNA was synthesized from 3 μg of total RNA treated with DNase using a Superscript II kit (Invitrogen Co., Carlsbad, CA). For semiquantitative reverse transcription-PCR (*PCDHB1-PCDHB15*), multiple cycles of PCR were tested for each gene, and numbers giving a wide dynamic range were determined. The primers and PCR conditions are shown in Supplementary Table 2. For quantitative reverse transcription-PCR (*PCDHB16*), the number of cDNA molecules was determined by quantitative PCR, as in quantitative MSP, and the copy number was normalized to that of *GAPDH*.

Chromatin Immunoprecipitation Assay. From 1×10^6 cells, DNA/histone complexes were immunoprecipitated, and DNA was eluted in 30 μL of TE after reversing cross-linking. Copy numbers of DNA molecules of the *PCDHB16* exon, *RASSF1A* promoter, and *GAPDH* promoter in 1 L of the eluate were determined by quantitative PCR (primer sequences in Supplementary Table 3), and normalized to the copy numbers in the input. Anti-acetyl-histone H3 antibody (AcH3) and anti-dimethylated-histone H3 (lysine 9; MetH3K9) were purchased from Cell Signalling (Beverly, MA).

Statistical Analysis. Associations between methylation levels among CGI groups were examined using the Pearson correlation coefficient and Fisher's exact test. Survival time was measured from the date of initial diagnosis to the date of death or last contact. Kaplan-Meier analysis and log-rank tests were done to compare survival between the groups defined by methylation levels. Hazard ratio (HR) between groups and dose-response relationships between methylation levels and survival were estimated by the Cox proportional hazard model. Kaplan-Meier curves were drawn with the help of Aabel software (Gigawiz. Ltd. Co., Tulsa, OK) and other analyses were conducted using SAS version 8.2 (SAS Institute, Inc., Cary, NC).

Results

Genome-Scanning for Differentially Methylated CpG Islands. MS-RDA was done using five primary neuroblastomas with a good prognosis and five neuroblastoma cell lines established from cases with a poor prognosis. Seven DNA fragments, derived from CGIs of *PCDHB16*, *PCDHA1*, *HLP*, *DKFZp451I127*, *FLJ37440*, *ZNF297*, and *CYP26C1*, were isolated as methylated in the latter samples. No DNA fragments were isolated as methylated in the former samples. Methylation statuses of (i) 17 CGIs of the *PCDHB* family (detailed structure in Supplementary Fig. 1), (ii) 13 CGIs of the *PCDHA* family, (iii) *HLP* and its pseudogene, and (iv) other four unique CGIs were examined by MSP. This revealed that the *PCDHB* family (5q31), the *PCDHA* family (5q31), *HLP* (3p21) and its pseudogene (1p36), *DKFZp451I127* (5q14), and *CYP26C1* (10q23) were specifically methylated in the latter samples (Fig. 1*A* and *B*).

Close Association between Methylation and Poor Prognosis in 140 Independent Primary Samples. To analyze the significance of the differential methylation of the above five CGI (groups) in primary neuroblastomas, 140 primary samples, all different from the initial five samples, were analyzed by quantitative MSP. When distributions of methylation indices were analyzed (Fig. 2), a clear bimodal distribution was observed for (i) the CGI group in the *PCDHB* family (17 CGIs), (ii) the CGIs of *HLP* and its pseudogene, and (iii) the *CYP26C1* CGI. The results thus indicated that the cases could be classified into two groups, one with high methylation and the other with low methylation. The dose-response relationships between high *PCDHB* methylation and poor prognosis were analyzed by the Cox proportional model using the methylation index as a continuous value, and the association was confirmed with a trend $P < 0.0001$. Normal adrenal medulla had a methylation index of 4%.

According to the bimodal distribution, the effect of high methylation was assessed by dichotomous groups. For the *PCDHB* family, cutoff values of 30%, 40%, 50%, 60%, 70%, and 80% were tested, and HRs of 16.8 [95% confidence interval (95% CI), 4.0-70.9], 22.1 (95% CI, 5.3-93.4; Fig. 3), 13.1 (95% CI, 4.5-37.9), 9.1 (95% CI, 3.8-23.4), 7.0 (95% CI, 3.1-15.8), and 7.8 (95% CI, 3.4-17.6), respectively, were obtained ($P < 0.001$ for all cutoff values). This showed that cases can be classified into two groups with distinct prognoses, and we adopted a cutoff value of 40%, which gave the highest HR, for convenience in the following analysis.

The dose-response relationships were also confirmed for other four CGI (groups), *PCDHA* ($P = 0.004$), *HLP* ($P < 0.0001$), *DKFZp451I127* ($P = 0.02$), and *CYP26C1* ($P < 0.0001$). Cutoff values were similarly tested, and those for *PCDHA*, *HLP*, *DKFZp451I127*, and *CYP26C1* were set at 80%, 10%, 20%, and 70%, respectively, with HRs of 5.7 (95%CI, 1.4-24.0; $P = 0.07$), 21.7 (95% CI, 5.1-91.4; $P < 0.0001$), 3.2 (95% CI, 1.0-10.5; $P = 0.045$), and 8.7 (95% CI, 4.1-18.1; $P < 0.0001$), respectively (Fig. 3).

Existence of the CpG Island Methylator Phenotype in Neuroblastomas. Methylation of the different CGI (groups) had shown close associations with each other (Table 1). When correlation was analyzed as a continuous value, Pearson correlation coefficients between *PCDHB* and *PCDHA*, *HLP*, *DKFZp451I127* and *CYP26C1* were 0.55, 0.70, 0.26 and 0.77, respectively. This showed that multiple CGIs were simultaneously methylated in

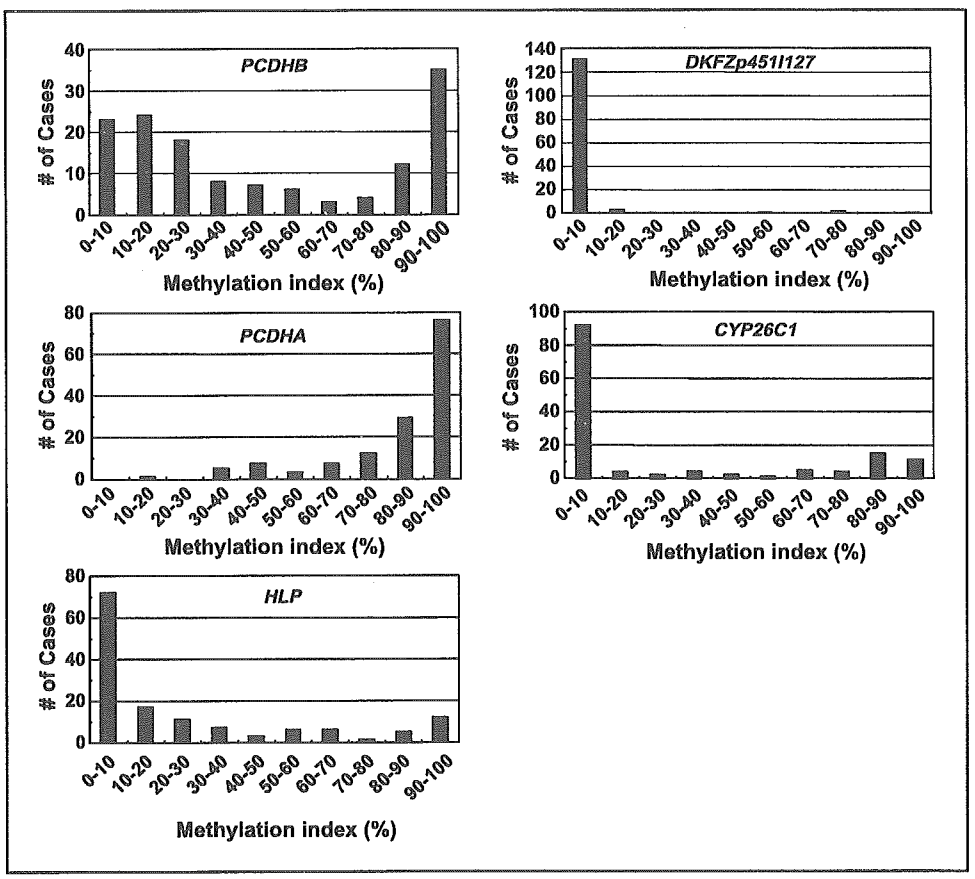

Figure 2. The distribution of methylation indices among the 140 cases analyzed: (*i*) 17 CGIs of the *PCDHB* family, (*ii*) 13 CGIs of the *PCDHA* family, (*iii*) CGIs of *HLP* and its pseudogene, (*iv*) *DKFZp451I127*, and (*v*) *CYP26C1*.

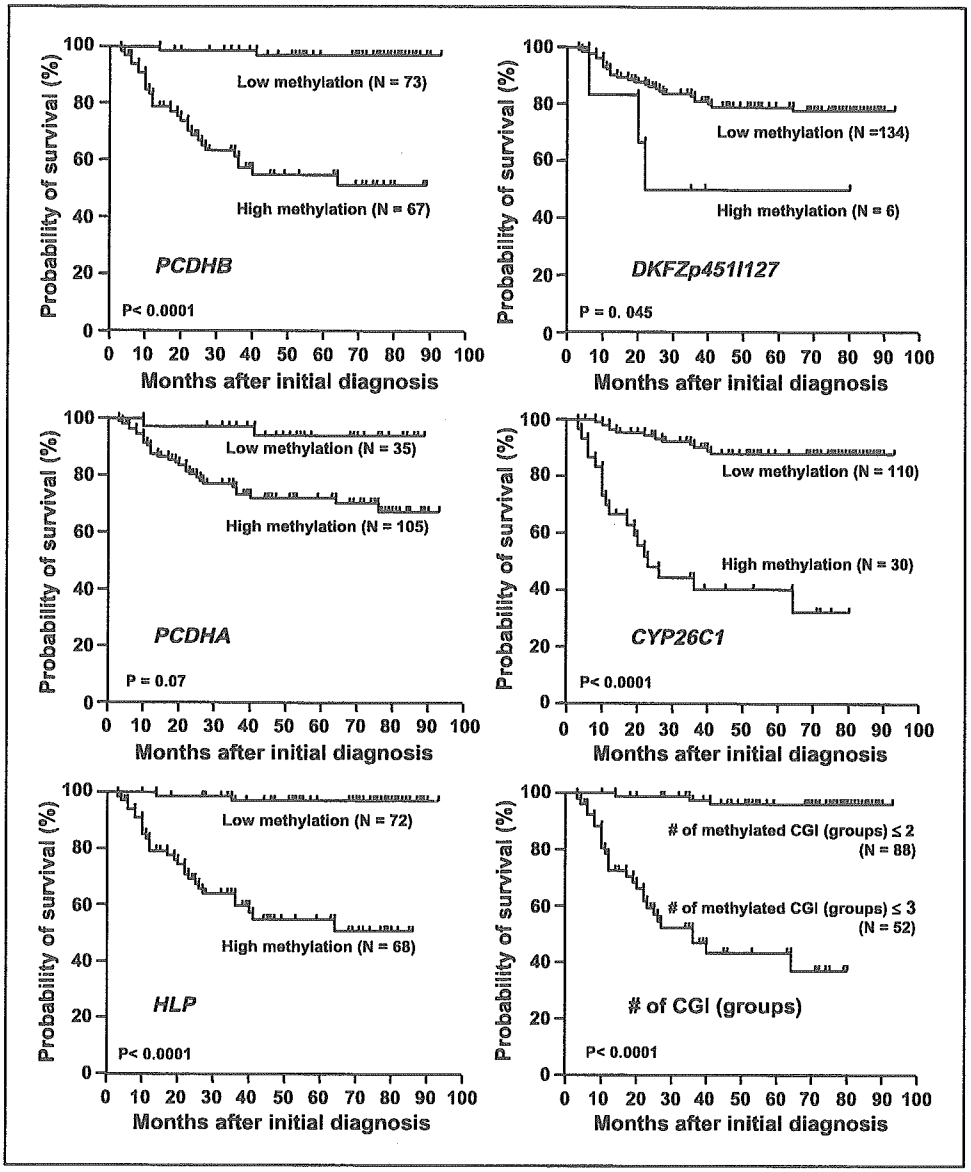

Figure 3. Predictive powers of methylation of the five CGI (groups) identified, and their multiple methylation: (*i*) 17 CGIs of the *PCDHB* family, (*ii*) 13 CGIs of the *PCDHA* family, (*iii*) CGIs of *HLP* and its pseudogene, (*iv*) *DKFZp451I127*, (*v*) *CYP26C1*, and (*vi*) methylation of three of these or more were analyzed by the Kaplan-Meier method using 140 primary samples. The *PCDHB* family, *HLP*, *DKFZp451I127*, *CYP26C1*, and methylation of multiple CGI (groups) had significant influence on survival.

neuroblastomas with a poor prognosis (Supplementary Fig. 2*A*). The simultaneous methylation of (i) 17 CGIs of the *PCDHB* family, (ii) 13 CGIs of the *PCDHA* family, (iii) CGIs of *HLP* and its pseudogene, (iv) *DKFZp451I127* CGI, and (v) *CYP26C1* CGI conformed with the concept of the CpG island methylator phenotype (CIMP; ref. 16).

Associations between CIMP and poor prognosis were examined by defining CIMP as cases with methylation of two CGI (groups) or more, those with three or more, those with four or five, and those with five. When CIMP was defined as cases with methylation of three CGI (groups) or more, the largest association with poor prognosis was observed, with a HR of 25.4 (95% CI, 7.6-84.5; Fig. 3). However, the HR (22.1) given by 17 CGIs of the *PCDHB* gene family approximated to this, and the *PCDHB* methylation level closely correlated with the number of methylated CGI (groups; Supplementary Fig. 2*B*). Therefore, for simplicity of analysis, we defined CIMP in neuroblastomas on the basis of high methylation of the *PCDHB* family, tentatively with a cutoff value of 40%.

Predictive Power of CIMP, Compared with Known Prognostic Factors. Univariate analyses showed that N-*myc* amplification, low *TrkA* expression, DNA diploidy, and an age no younger than 1 year gave HRs of 9.5 (95% CI, 4.4-20.5), 3.9 (95% CI, 1.7-9.3), 4.2 (95% CI, 1.65-10.8), and 12.3 (95% CI, 3.7-41.7). Cases were stratified by these known factors (Table 2). In those without N-*myc* amplification, CIMP also showed an influence with a HR of 12.4 (95% CI, 2.6-58.9), but almost all cases with N-*myc* amplification (37 of the 38 cases) showed CIMP. It was suggested that cases with N-*myc* amplification were contained in the cases with CIMP. CIMP was independent from *TrkA* overexpression, DNA ploidy, and age at diagnosis. Stage seemed to be a stronger prognostic factor. Notably, even when limited to cases in stages III and IV without N-*myc* amplification, which are classified into the intermediate risk group and clinically important, CIMP gave a HR of 4.8 (95% CI, 1.0-23.0; $P = 0.048$).

Multivariate analyses were finally done taking all the five known prognostic factors into account. Although CIMP gave a HR of 5.0 (95% CI, 0.47-52.7), it was not significant ($P = 0.18$), possibly due to limitation in the number of cases.

Table 1. Association between the *PCDHB* methylation and methylation of other CGIs

Variables	Methylation level of *PCDHB* family gene		*P**
	High (≥40%)	Low (<40%)	
No. cases (n = 140)	67	73	
Methylation of CGIs outside promoter regions (n = 140)			
PCDHA gene family (exon 1)†	65/67	41/73	<0.0001
HLP (exons 2-13)‡	52/67	16/73	<0.0001
CYP26C1 (exon 2)§	30/67	0/73	<0.0001
p41Arc (intron 8)	1/67	1/73	0.48
SIM2 (exon 2)	0/67	0/73	
Methylation of CGIs in promoter regions (n = 140)			
DKFZp451I127‖	6/67	0/73	0.011
RASSF1A	51/67	10/73	<0.0001
BLU	25/67	3/73	<0.0001
p16	0/67	0/73	
hMLH1	0/67	0/73	
PCDHB1	0/67	0/73	
TAF7	0/67	0/73	
p41Arc	0/67	0/73	
SIM2	0/67	0/73	

*Fisher's exact test.
†Boundaries for high methylation and low methylation of *PCDHA* gene family were set at 80% of the methylation index.
‡Boundaries for high methylation and low methylation of *HLP* were set at 10% of the methylation index.
§Boundaries for high methylation and low methylation of *CYP26C1* were set at 70% of the methylation index.
‖Boundaries for high methylation and low methylation of *DKFZp451I127* were set at 20% of the methylation index.

Effects of PCDHB Methylation on Gene Expression and Chromatin Structure. The CGIs of the *PCDHB* family were located in their gene bodies, whose methylation generally does not block gene transcription (17). The actual effects of methylation on expression were examined for 16 genes of the *PCDHB* family using 10 primary neuroblastomas with low methylation and five primary neuroblastomas with high methylation. The methylation was not associated with loss of expression (a representative result is shown in Fig. 4*A*). The effect of methylation of the *PCDHB16* CGI on the histone modification was further examined by chromatin immunoprecipitation assay. It was found that DNA methylation of the *PCDHB16* CGI did not induce histone H3 lysine 9 methylation or histone H3 deacetylation (data not shown).

Association between CIMP and Promoter Methylation. High methylation of *PCDHB* CGIs, a sensitive surrogate marker of CIMP in neuroblastomas, did not repress gene expression or induce histone modification. This indicated that CIMP is involved in the poor prognosis of neuroblastomas by causing methylation of promoter CGIs, although it is known that promoter CGIs are resistant to *de novo* methylation (18, 19).

Among the five CGI (groups) identified in this study, only that of *DKFZp451I127* was located in a promoter region. Although its methylation was infrequent, the methylation was observed only in neuroblastomas with CIMP (Table 1), and was associated with expression loss (Fig. 4*B*). To make the association clearer, methylation statuses were analyzed for eight additional CGIs in promoter regions. It was shown that methylation of promoter CGIs of *RASSF1A* (3p21) and *BLU* (3p21) was far more frequently observed in neuroblastomas with CIMP (Table 1, $P < 0.0001$). At the same time, there was a preference for CGIs affected by CIMP among CGIs in promoter regions, and also among those outside promoter regions (Table 2).

Discussion

Extensive methylation of multiple CGIs, conforming with the concept of CIMP, was here found specifically present in neuroblastomas with a poor prognosis and could be sensitively detected by focusing on the *PCDHB* family. *PCDHB* methylation did not suppress gene expression or induce histone modification. However, CIMP was associated with promoter methylation of *RASSF1A* and *BLU* genes and one of the mechanisms underlying the poor prognosis of neuroblastomas seemed to be silencing of these and possibly other tumor suppressor genes and genes important for differentiation.

CIMP was originally identified in colon cancers (16), but there has been some dispute over its presence (20). The clear correlation between CIMP and a poor prognosis found here for neuroblastomas was unequivocal and presumably reflects an intrinsic tendency for methylation of CGIs. This is because, first, neuroblastomas have a much shorter history than colon cancers, and the accumulated number of methylated CGIs in neuroblastomas is expected to parallel the speed of occurrence of

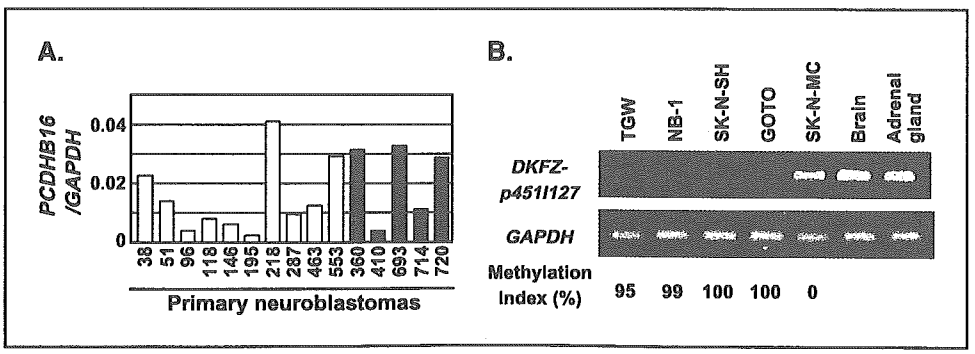

Figure 4. Effects of methylation of the *PCDHB* family and *DKFZp451I127* on gene expression. *A*, *PCDHB16* expression was analyzed by quantitative RT-PCR in 10 primary samples with low methylation (*open columns*) and five primary samples with high methylation (*closed columns*), and no difference was observed between the two groups. *B*, silencing of *DKFZp451I127* by methylation of its promoter CGI. The CGI was methylated in four cell lines, TGW, NB-1, SK-N-SH, and GOTO, whereas it was unmethylated in one cell line, SK-N-MC. *DKFZp451I127* was expressed in SK-N-MC, but not expressed at all in the four cell lines with the promoter methylation.

Table 2. HRs of death by *PCDHB* methylation status in subgroup of known prognostic factors

Stratified by		*PCDHB* methylation	No. cases	No. deaths	HR* (95% CI)	$P^{\dagger}$
Overall (n = 140)		High	67	1	22.1 (5.3-93.4)	< 0.0001
		Low	73	2	1	
N-*myc* amplification (n = 140)	No	High	30	8	12.4 (2.6-58.9)	0.002
		Low	72	2	1	
	Yes	High	37	20	NE	—
		Low	1	0		
TrkA overexpression (n = 130)	Yes	High	20	6	18.3 (2.2-152.6)	0.007
		Low	49	1	1	
	No	High	40	19	NE	
		Low	21	0		
DNA ploidy (n = 125)	Aneuploid	High	17	5	18.3 (2.1-156.7)	0.008
		Low	49	1	1	
	Diploid	High	38	17	NE	
		Low	21	0		
Clinical stages (n = 140)	Stages I, II, and IVS	High	8	0	NE	—
		Low	52	0		
	Stages III and IV	High	59	28	7.4 (1.8-31.3)	0.006
		Low	21	2	1	
Age at diagnosis (n = 140)	<1	High	11	3	NE	
	≥1	Low	59	0		
		High	56	25	4.5 (1.1-18.9)	0.043
		Low	14	2	1	

*HR of death for a case with high *PCDHB* methylation compared with a case with low methylation. NE shows not estimable due to no events in at least one category.
†Significance level for a high *PCDHB* methylation to low methylation using Cox proporitonal model.

methylation. Second, methylation of the *PCDHB* family did not affect gene expression, and there should have been no selection of cells with the *PCDHB* methylation, in contrast to the case of promoter methylation of tumor suppressor genes. Investigation into the mechanism of the intrinsic tendency for methylation of multiple CGIs is necessary. Furthermore, alleviation of the intrinsic tendency could block progression of neuroblastomas and have potential therapeutic value.

Among the six CGI (groups) outside promoter regions analyzed here, CIMP in neuroblastomas preferentially affected four CGI (groups); those of the *PCDHB* family, the *PCDHA* family, *HLP*, and *CYP26C1*. Unexpectedly, three CGIs that are known to be frequently methylated in human colon cancers with CIMP, MINT1, MINT2, and MINT17 (16) were not methylated in neuroblastoma cell lines (data not shown). Among the nine CGIs in promoter regions analyzed, CIMP in neuroblastomas affected only three, those of *RASSF1A*, *BLU*, and *DKFZp451I127*. The nine CGIs were selected based upon previous reports as tumor suppressor genes (*RASSF1A*, *BLU*, *p16*, and *hMLH1*; refs. 21–23), the chromosomal location flanking the *PCDHB* family (*PCDHB1* and *TAF7*), our previous report on the fidelity in inheriting methylation patterns (*p41Arc* and *SIM2*; ref. 19), and the findings here (*DKFZp451I127*). Because gene expression and possibly chromatin structures affect the frequency of *de novo* methylation (24, 25), the available data suggest that CGIs useful to sensitively detect CIMP might vary according to the tumor type.

The influence of CIMP on prognosis was here found to be comparable to that of the currently most reliable marker, N-*myc* amplification, and stronger than *TrkA* overexpression and DNA ploidy on univariate analysis. Subgroup analysis showed that the influence was independent of *TrkA* overexpression, DNA ploidy and age at diagnosis and CIMP had influence even in cases without N-*myc* amplification and in advanced stages. These points strongly indicated CIMP to be a promising new prognostic marker. However, the cutoff values adopted here are tentative, and the HRs obtained could have been overestimated. A validation study using independent samples is necessary for further evaluation. The fact that cases with CIMP contained almost all the cases with N-*myc* amplification suggested that a common molecular mechanism caused both alterations, or that CIMP may lead to N-*myc*

amplification. Whatever the case, the findings might provide clues to molecular mechanisms of neuroblastoma development.

In summary, the present study showed that CIMP is present specifically in neuroblastomas with poor prognosis and that can be sensitively detected by focusing on *PCDHB* methylation. CIMP seems to be a promising new prognostic marker, and its evaluation and investigations into the mechanisms underlying CIMP in neuroblastomas seem warranted.

Acknowledgments

Received 7/27/2004; revised 11/14/2004; accepted 11/24/2004.

Grant support: Grant-in-aid for the Third-term Cancer Control Strategy Program from the Ministry of Health, Labour, and Welfare, Japan and Research Resident Fellowship from the Foundation for Promotion of Cancer Research (M. Abe).

The costs of publication of this article were defrayed in part by the payment of page charges. This article must therefore be hereby marked advertisement in accordance with 18 U.S.C. Section 1734 solely to indicate this fact.

We thank Drs. E. Okochi-Takada and G. S. Goldberg for critical reading of the article and the institutions for participation in the collection of clinical materials.

References

1. Jones PA, Baylin SB. The fundamental role of epigenetic events in cancer. Nat Rev Genet 2002;3:415–28.
2. Chen RZ, Pettersson U, Beard C, Jackson-Grusby L, Jaenisch R. DNA hypomethylation leads to elevated mutation rates. Nature 1998;395:89–93.
3. Kondo Y, Kanai Y, Sakamoto M, et al. Genetic instability and aberrant DNA methylation in chronic hepatitis and cirrhosis-A comprehensive study of loss of heterozygosity and microsatellite instability at 39 loci and DNA hypermethylation on 8 CpG islands in microdissected specimens from patients with hepatocellular carcinoma. Hepatology 2000;32:970–9.
4. Ushijima T, Morimura K, Hosoya Y, et al. Establishment of methylation-sensitive-representational difference analysis and isolation of hypo- and hypermethylated genomic fragments in mouse liver tumors. Proc Natl Acad Sci U S A 1997;94:2284–9.
5. Kaneda A, Takai D, Kaminishi M, Okochi E, Ushijima T. Methylation-sensitive representational difference analysis and its application to cancer research. Ann N Y Acad Sci 2003;983:131–41.
6. Takai D, Yagi Y, Wakazono K, et al. Silencing of *HTR1B* and reduced expression of *EDN1* in human lung cancers, revealed by methylation-sensitive representational difference analysis. Oncogene 2001; 20:7505–13.
7. Kaneda A, Kaminishi M, Yanagihara K, Sugimura T, Ushijima T. Identification of silencing of nine genes in human gastric cancers. Cancer Res 2002;62:6645–50.
8. Miyamoto K, Asada K, Fukutomi T, et al. Methylation-associated silencing of heparan sulfate *D-glucosaminyl 3-O-sulfotransferase-2* (*3-OST-2*) in human breast, colon, lung and pancreatic cancers. Oncogene 2003;22:274–80.
9. Hagihara A, Miyamoto K, Furuta J, et al. Identification of 27 5′ CpG islands aberrantly methylated and 13 genes silenced in human pancreatic cancers. Oncogene 2004;23:8705–10.
10. Brodeur GM. Neuroblastoma: biological insights into a clinical enigma. Nat Rev. Cancer 2003;3:203–16.
11. Schwab M, Westermann F, Hero B, Berthold F. Neuroblastoma: biology and molecular and chromosomal pathology. Lancet Oncol 2003;4:472–80.
12. Nakagawara A, Arima-Nakagawara M, Scavarda NJ, et al. Association between high levels of expression of the *TRK* gene and favorable outcome in human neuroblastoma. N Engl J Med 1993;328:847–54.
13. Jaenisch R, Bird A. Epigenetic regulation of gene expression: how the genome integrates intrinsic and environmental signals. Nat Genet 2003;33:245–54.
14. Li E. Chromatin modification and epigenetic reprogramming in mammalian development. Nat Rev Genet 2002;3:662–73.
15. Kaneda A, Kaminishi M, Sugimura T, Ushijima T. Decreased expression of the seven ARP2/3 complex genes in human gastric cancers. Cancer Lett 2004; 212:203–10.
16. Toyota M, Ahuja N, Ohe-Toyota M, et al. CpG island methylator phenotype in colorectal cancer. Proc Natl Acad Sci U S A 1999;96:8681–6.
17. Gonzalgo ML, Hayashida T, Bender CM, et al. The role of DNA methylation in expression of the *p19/p16* locus in human bladder cancer cell lines. Cancer Res 1998;58:1245–52.
18. Nguyen C, Liang G, Nguyen TT, et al. Susceptibility of nonpromoter CpG islands to *de novo* methylation in normal and neoplastic cells. J Natl Cancer Inst 2001; 93:1465–72.
19. Ushijima T, Watanabe N, Okochi E, et al. Fidelity of the methylation pattern and its variation in the genome. Genome Res 2003;13:868–74.
20. Yamashita K, Dai T, Dai Y, Yamamoto F, Perucho M. Genetics supersedes epigenetics in colon cancer phenotype. Cancer Cell 2003;4:121–31.
21. Agathanggelou A, Dallol A, Zochbauer-Muller S, et al. Epigenetic inactivation of the candidate 3p21.3 suppressor gene *BLU* in human cancers. Oncogene 2003; 22:1580–8.
22. Takita J, Hayashi Y, Nakajima T, et al. The *p16* (*CDKN2A*) gene is involved in the growth of neuroblastoma cells and its expression is associated with prognosis of neuroblastoma patients. Oncogene 1998; 17:3137–43.
23. Harada K, Toyooka S, Maitra A, et al. Aberrant promoter methylation and silencing of the *RASSF1A* gene in pediatric tumors and cell lines. Oncogene 2002; 21:4345–9.
24. De Smet C, Loriot A, Boon T. Promoter-dependent mechanism leading to selective hypomethylation within the 5′ region of gene *MAGE-A1* in tumor cells. Mol Cell Biol 2004;24:4781–90.
25. Richards EJ, Elgin SC. Epigenetic codes for heterochrómatin formation and silencing: rounding up the usual suspects. Cell 2002;108:489–500.

Oncogene (2005) 24, 3385–3396

www.nature.com/onc

ORIGINAL PAPERS

topors, a p53 and topoisomerase I-binding RING finger protein, is a coactivator of p53 in growth suppression induced by DNA damage

Ling Lin[1,2,3], Toshinori Ozaki[4], Yuki Takada[1,2], Hajime Kageyama[4], Yoko Nakamura[4], Akira Hata[5], Jian-Hua Zhang[3], William F Simonds[3], Akira Nakagawara[4] and Haruhiko Koseki*[,1,2]

[1]*Department of Molecular Embryology, Graduate School of Medicine, Chiba University, 1-8-1 Inohana, Chuo-ku, Chiba 260-8670, Japan;* [2]*RIKEN Research Center for Allergy and Immunology, RIKEN Yokohama Institute, 1-7-22 Suehiro, Tsurumi-ku, Yokohama 230-0045, Japan;* [3]*Metabolic Diseases Branch, National Institute of Diabetes, Digestive and Kidney Diseases, NIH, Bethesda, MD 20892, USA;* [4]*Division of Biochemistry, Chiba Cancer Center Research Institute, 666-2 Nitona, Chuoh-ku, Chiba 260-8717, Japan;* [5]*Department of Public health, Graduate School of Medicine, Chiba University, 1-8-1 Inohana, Chuo-ku, Chiba 260-8670, Japan*

The RING family zinc-finger protein topors (topoisomerase I-binding protein) binds not only topoisomerase I, but also p53 and the AAV-2 Rep78/68 proteins. topors maps to human chromosome 9p21, which contains candidate tumor suppressor genes implicated in small cell lung cancers. In this study, we isolated the murine counterpart of topors and investigated its impact on p53 function. The deduced amino-acid sequence of mouse topors exhibits extensive similarity to human topors. Overexpressed myc-tagged topors associates with and stabilizes p53, and enhances the p53-dependent transcriptional activities of *p21^{Waf1}*, *MDM2* and *Bax* promoters and elevates endogenous *p21^{Waf1}* mRNA levels. Overexpression of topors consequently results in the suppression of cell growth by cell cycle arrest and/or by the induction of apoptosis. Taken together, these studies identify topors as a positive regulator of p53. The expression of *topors* is induced by exposure to the genotoxic reagents cisplatin and camptothecin, a DNA topoisomerase I inhibitor. We therefore postulate that topors mediates p53-dependent cellular responses induced by DNA damage, suggesting its physiological role as a tumor suppressor.
Oncogene (2005) **24,** 3385–3396. doi:10.1038/sj.onc.1208554
Published online 28 February 2005

Keywords: topors; p53; tumor suppressor; DNA damage; cell cycle; apoptosis

Introduction

The p53 tumor suppressor protein is defined as the guardian of the genome, and more than half of all human cancers are characterized by either the loss of the p53 protein or by mutations in its gene (Lane, 1992; Ko and Prives, 1996). The p53 protein comprises 393 amino acids including an amino-terminal transactivation domain, a sequence-specific DNA-binding domain and a multifunctional carboxyl-terminal domain. p53 is involved in the regulation of the cell cycle, apoptosis, senescence, DNA repair, cell differentiation and angiogenesis (Levine, 1997; Vogelstein *et al.*, 2000). These activities of p53 are mediated by one or more known mechanisms including the transcriptional regulation of target genes, functional regulation of interacting proteins, DNA annealing and exonuclease activity. p53 is activated by several stress conditions including DNA damage, the expression of several oncogene products, changes in cellular adhesion and redox potential, and reduction in the ribonucleoside triphosphate pool. In response to such stress signals, p53 undergoes extensive post-translational modification that modulates its stability and activity. The stabilization of p53 is presumed to play a major role in its activation, while modifications unrelated to p53 stabilization may regulate its specific activity (Sionov and Haupt, 1999; Vogelstein *et al.*, 2000). The stability of p53 is tightly regulated by multiple positive and negative feedback loops involving a number of p53 interacting proteins (Sionov and Haupt, 1999; Vogelstein *et al.*, 2000).

Human topoisomerase I-binding protein (h-topors) was first identified by yeast two-hybrid screening as a protein that interacts with human topoisomerase I (hTop1), and turned out to be identical to a novel p53-binding protein, p53BP3 (Haluska *et al.*, 1999; Zhou *et al.*, 1999). An identical protein was also isolated as the DNA-binding protein LUN, as a protein that interacts with adeno-associated virus type 2 (AAV-2) Rep78/68 proteins and as a protein binding to the interferon-inducible large GTPase Mx1 (Chu *et al.*, 2001; Engelhardt *et al.*, 2001; Weger *et al.*, 2002). h-topors is predicted to contain 1045 amino acids and to encode a RING family zinc-finger domain, a putative leucine zipper (LZ) domain, five sequences rich in proline, glutamine, serine and threonine (PEST sequences), an arginine/serine-rich (RS) domain and a bipartite nuclear localization signal (NLS). h-topors is

*Correspondence: H Koseki, RIKEN Research Center for Allergy and Immunology, RIKEN Yokohama Institute, 1-7-22 Suehiro, Tsurumi-ku, Yokohama 230-0045, Japan; E-mail: koseki@rcai.riken.jp
Received 1 June 2004; revised 18 January 2005; accepted 18 January 2005; published online 28 February 2005

modified by conjugation to the small ubiquitin-like modifier, SUMO-1 (Weger *et al.*, 2003), and both endogenous h-topors and overexpressed h-topors-GFP fusion protein are mainly distributed in promyelocytic leukemia-associated protein (PML) nuclear bodies in a PML protein-dependent fashion (Rasheed *et al.*, 2002). The carboxyl-terminal region of h-topors is required for such punctate nuclear localization (Rasheed *et al.*, 2002). In addition, the amino-terminal region of h-topors, containing the RING zinc-finger motif and LZ region, has been shown to bind to DNA in a sequence-specific as well as Zn^{2+}-dependent manner (Chu *et al.*, 2001). Since h-topors enhances the expression of a Rep78/68-dependent AAV-2 gene in the absence of helper virus, h-topors might be a transcriptional regulator (Weger *et al.*, 2002).

Although h-topors interacts with p53 as revealed by yeast two-hybrid assay, the role of h-topors in regulating the function of p53 remains to be clarified (Zhou *et al.*, 1999; Weger *et al.*, 2002). Several lines of evidence suggest that h-topors might be an important regulator in cell proliferation. Relocalization of topors in cells exposed to the Topl-targeting drug camptothecin (CPT) or the transcription inhibitor 5,6-dichloro-1-β-D-ribofuranolsylbenzimidazole (DRB) suggests its involvement in mediating the DNA damage response induced by CPT or DRB, which have been shown to cause an accumulation of p53 (Klibanov *et al.*, 2001; Rasheed *et al.*, 2002). h-topors interacts with AAV-2 Rep78, which has been proved to be an effective repressor of the adenovirus in the process of tumor generation (Schlehofer, 1994). Intriguingly, the region of h-topors required for interaction with AAV-2 Rep78/68 overlaps with that for p53 binding, as revealed by yeast two-hybrid analysis (Batchu *et al.*, 1999; Weger *et al.*, 2002). In addition, h-topors maps to chromosome 9p21, a locus containing candidate tumor suppressor gene(s) associated with the loss of heterozygosity in 86% of small cell lung cancers (Chu *et al.*, 2001). These observations prompted us to examine the functional role of topors in the regulation of p53. In the present study, we describe a physical and functional interaction between mouse topors and p53 in mammalian cultured cells. Our results strongly suggest that topors acts as a coactivator of p53 in response to DNA damage.

Results

Identification of a murine counterpart of topors

To identify proteins that interact with the Polycomb group (PcG) protein Mph2 (Yamaki *et al.*, 2002), we employed yeast-based two-hybrid screening using a cDNA library derived from mouse embryo and bait derived from full-length Mph2. We isolated two identical 1.2-kb cDNA fragments encoding a polypeptide highly homologous to the carboxyl-terminal half of h-topors. By conventional cDNA screening of a mouse brain cDNA library and database screening, two overlapping clones, a 3.5-kb fragment lacking the amino-terminal region and a mouse EST clone lacking the carboxyl-terminal region, were isolated. The nucleotide sequences of both clones were determined, and the combined nucleotide sequences revealed the longest open reading frame (ORF) of 1033 amino-acid residues with 86% overall identity to h-topors (DDBJ accession number: AB104865). In the amino-terminal region, a RING family zinc-finger domain and an LZ region exhibited 100 and 98% homology to h-topors, respectively (red letters and open blue box in Figure 1a, respectively). The p53-binding domains of h-topors were previously shown to be separated into two blocks based on yeast two-hybrid interactions (underlined in Figure 1a) (Zhou *et al.*, 1999; Weger *et al.*, 2002). A bipartite NLS was present in the amino-terminal block of the p53-binding domains (blue letters in Figure 1a). A cluster of residues including the two p53-binding subdomains and an intermediate region exhibited 90% identity with h-topors (Figure 1b). Because of the extensive similarity to h-topors, this newly isolated cDNA was identified as a murine counterpart of the *h-topors* gene. The mouse *topors* gene was mapped to a 40 Mb region of mouse chromosome 4 by BLAST analysis of the mouse genome (40017898–40007704 bp; Ensemble Mouse Genome Browser), a region syntenic to human chromosome 9p21. This chromosomal localization is in agreement with a previous report in which human *topors* was mapped to the chromosome 9p21 region (Chu *et al.*, 2001).

h-topors has been shown to associate with PML nuclear bodies in exponentially growing HeLa cells (Rasheed *et al.*, 2002). To examine the subcellular localization of mouse topors in mammalian cultured cells, we constructed an expression vector encoding myc-epitope-tagged topors (myc-topors) and confirmed its expression by *in vitro* transcription/translation experiments as well as transient transfection into COS-7 cells (Figure 1c and d). Consistent with the previous observation, myc-topors migrated more slowly (195 kDa) than predicted based on the calculated molecular mass, which has been suggested to be due to the phosphorylation of serine residues in the RS domain (Haluska *et al.*, 1999). The subcellular localization of myc-topors was also examined in U2-OS cells by transient overexpression. In interphase nuclei of morphologically intact transfectants, the myc-topors protein was always localized in the nuclei. Two types of transfectants were reproducibly observed. One type exhibited a fine speckled distribution to form 10–20 foci and the other type showed larger, closely spaced dots with much stronger fluorescence in the nucleoplasm but excluded from the nucleolus (data not shown). These findings were identical to those of Haluska *et al.* (1999), who described the subcellular localization of a GFP fusion with h-topors in HeLa cells.

topors interacts with p53 and enhances p53-dependent transcription in mammalian cultured cells

The putative p53-binding domains revealed by yeast two-hybrid interaction (Zhou *et al.*, 1999; Weger *et al.*,

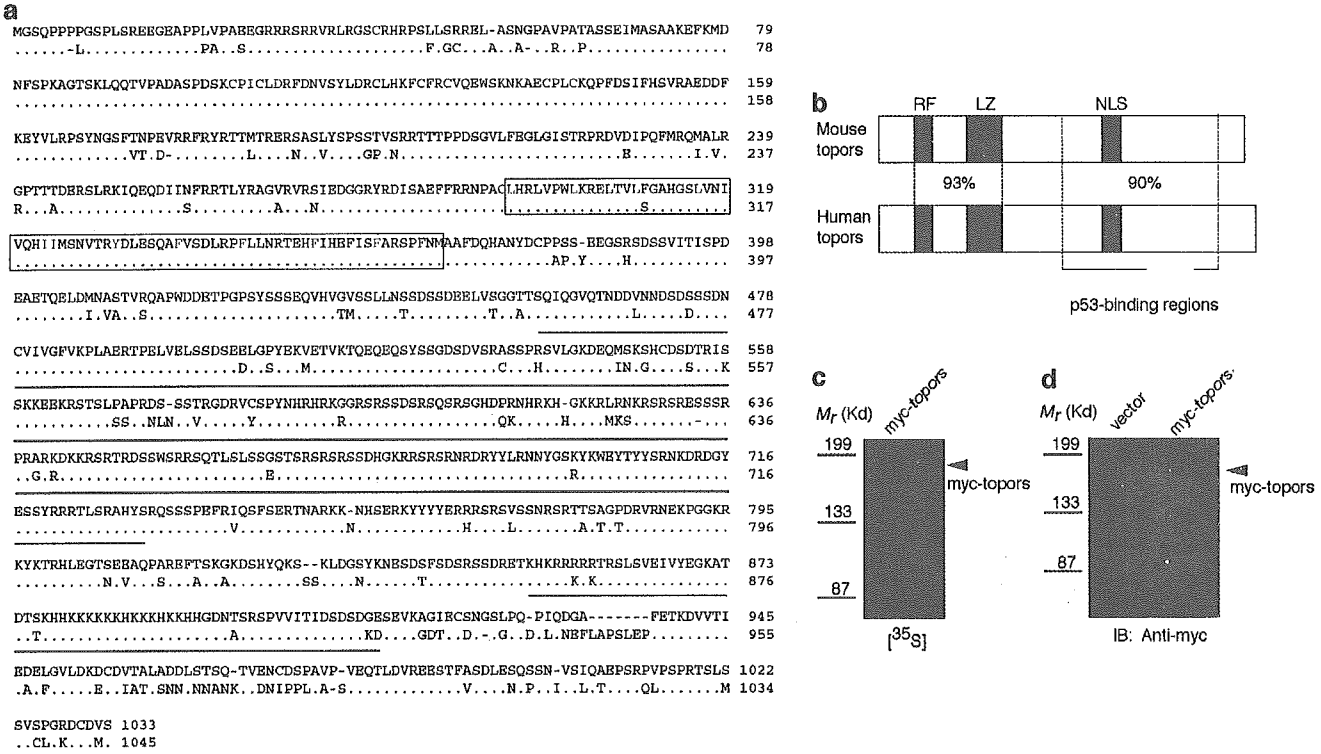

Figure 1 Amino-acid sequence, putative domain structure and expression of murine topors protein. (**a**) The deduced amino-acid sequence of mouse topors protein along with the sequence of the human counterpart. The sequences of mouse (top) and human (bottom) topors were aligned to provide the highest homology. Identical amino-acid residues are shown as dots in the human sequence; gaps are indicated by bars. Amino-acid residues in the putative RING finger motif and bipartite NLS are shown in red and blue letters, respectively. The region of the putative LZ structure is boxed with the hydrophobic residues at the first position of the heptad repeat shown in green letters. Two separate regions encoding putative p53-binding domains are underlined in red (see text). (**b**) Schematic representation of homologous domain structure shared between mouse and human topors. The RING finger motif (RF), LZ and bipartite NLS are indicated by red, green and blue boxes, respectively. Identical amino acids in each region are shown. (**c**) The myc-*topors* gene product generated by *in vitro* transcription/translation and analysed as described in Materials and methods. Relative molecular weight is indicated. (**d**) The myc-topors protein transiently overexpressed in COS-7 cells. Whole-cell lysates prepared from COS-7 cells transfected with either empty pcDNA3 (Vector, left) or pcDNA3-myc-*topors* (myc-*topors*, right) were subjected to immunoblotting analysis using the anti-myc monoclonal antibody

2002) are highly conserved between human and mouse topors (Figure 1a and b). This prompted us to examine whether myc-topors could interact with p53 in mammalian cultured cells. COS-7 cells were transiently transfected with myc-topors, and whole-cell extracts of the transfectants were subjected to immunoprecipitation with anti-p53 or normal mouse serum (NMS). As shown in Figure 2a, the anti-p53, but not the NMS, immunoprecipitates contained significant amounts of myc-topors, indicating that overexpressed myc-topors could associate with endogenous p53. This finding is consistent with the previous yeast two-hybrid studies demonstrating topors–p53 interaction (Zhou *et al.*, 1999; Weger *et al.*, 2002). We next addressed whether the physical interaction of topors with p53 might affect the function of p53. To this end, we examined the effects of overexpressed myc-topors on the p53-dependent transcription of *Bax*, *p21^{Waf1}* and *MDM2* promoters using luciferase assays in transiently transfected p53-deficient SAOS-2 and H1299 cells (Barak *et al.*, 1993; el-Deiry *et al.*, 1993; Miyashita and Reed, 1995). As shown in Figure 2b, the overexpression of myc-topors in SAOS-2 cells significantly enhanced p53-dependent transcription of the *Bax* and *MDM2* promoters in a dose-dependent manner. While myc-topors enhanced the p53-dependent activity of the *p21^{Waf1}* promoter in SAOS-2 cells, this effect did not achieve statistical significance (Figure 2b, middle panel). Similar results were obtained in H1299 cells, except that its effect on all three p53-responsive promoters was statistically significant as compared with p53 alone (Figure 2c). Under our experimental conditions, myc-topors alone had no effects on the *Bax*, *p21^{Waf1}* or *MDM2* promoter activity. We further studied whether the overexpression of topors influenced the expression of endogenous p53-regulated transcripts by quantitative real-time RT–PCR analysis of human *p21^{Waf1}* mRNA levels. As shown in Figure 2d and e, forced expression of topors enhanced the transcription of the p53 downstream gene *p21^{Waf1}* in both human small cell lung cancer SBC3 cells and U2-OS cells. Taken together, the results indicate that overexpression of topors enhances the sequence-specific transcriptional activity of p53 in a p53-dependent manner.

topors suppresses cell growth in a p53-dependent manner

These observations prompted us to investigate further whether the overexpression of myc-topors influences the growth suppression mediated by p53. For this purpose, we performed a colony formation assay using H1299 cells (lacking endogenous p53) and U2-OS cells containing the wild-type *p53* allele. The overexpression of myc-topors did not affect colony number in H1299 cells, while the colony number was significantly reduced in a dose-dependent manner in U2-OS cells (Figure 3a and b). The forced expression of p53 significantly reduced the colony number in H1299 cells, and this p53-dependent reduction was further intensified by cotransfection of pcDNA3-myc-*topors* (Figure 3a). Thus, the overexpression of topors appears to enhance the p53-dependent growth suppression of tumor cells.

In different systems, p53 can induce apoptosis or cause cell cycle arrest (Ko and Prives, 1996; Vogelstein *et al*., 2000). Because topors was able to enhance p53-dependent growth suppression, we next examined whether topors-dependent growth suppression involves apoptosis. The number of apoptotic cells exhibiting nuclear condensation and fragmentation was counted 48 h after transfection with either pcDNA3-myc-*topors* or pEGFP (Figure 3c-I–III). The number of apoptotic cells increased significantly among U2-OS cells overexpressing myc-topors compared to pEGFP transfectants (Figure 3c-IV). Thus, the growth suppression resulting from overexpression of topors may result in part from induction of apoptosis.

Since p53 activation is known to cause not only apoptosis but also cell cycle arrest, we next examined the impact of overexpressed myc-topors on cell cycle progression. For this purpose, we established stable cell lines overexpressing myc-topors. U2-OS cells were transfected with pcDNA3-myc-*topors*, and G418-resistant clones were individually isolated and screened for myc-topors expression by immunofluorescent staining. Two cell lines out of 200 clones screened were found to express myc-topors (*topors* sta-1 and *topors* sta-2), and *topors* sta-1 expressed myc-topors at a higher level than *topors* sta-2 (Figure 4a). In both of the stable transfectants, myc-topors exhibited a speckled nuclear distribution to form 10–20 foci (Figure 4b), as did endogenous mouse topors in NIH 3T3 fibroblasts (data not shown) and as reported for endogenous human topors (Rasheed *et al*., 2002). *topors* sta-1 and *topors* sta-2 cells displayed a significantly slower growth rate

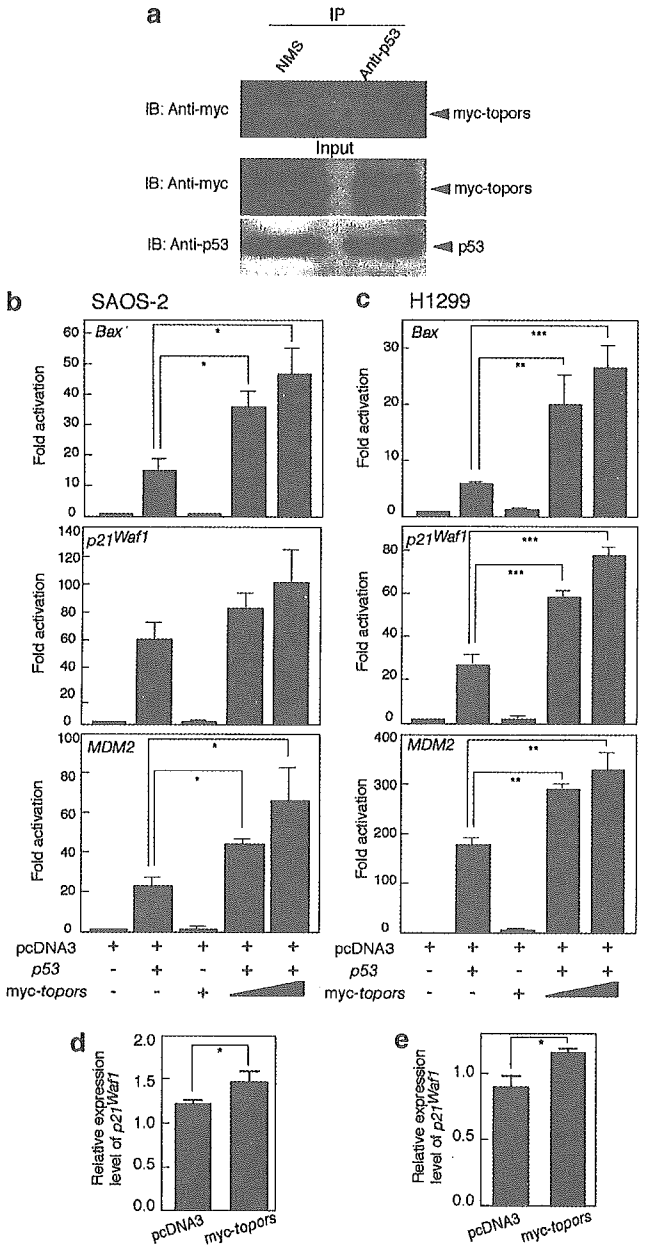

Figure 2 topors associates with p53 and activates p53-dependent transcription. (**a**) Association of transiently overexpressed myc-topors with endogenous p53 is shown by immunoprecipitation and subsequent immunoblotting analysis. (top) Whole-cell extract of COS-7 cells transfected with pcDNA3-myc-*topors* was subjected to immunoprecipitation with either NMS (left) or anti-p53 monoclonal antibodies (right) followed by immunoblotting with anti-myc monoclonal antibody. (middle and bottom) Unfractionated whole-cell extract of COS-7 cells transfected with myc-*topors* was subjected to immunoblotting using anti-myc monoclonal antibody (middle) or anti-p53 monoclonal antibody (bottom). (**b**, **c**) p53-deficient SAOS-2 (**b**) and H1299 (**c**) cells were transiently cotransfected with the expression plasmid for p53 along with luciferase reporter constructs containing the *Bax* (top), $p21^{Waf1}$ (middle) or *MDM2* (bottom) promoters in the presence or absence of increasing amounts of transfected pcDNA3-myc-*topors*. Transfection efficiency was standardized against *Renilla* luciferase. The average relative luciferase activities in triplicate experiments are represented as bars. Results are shown as fold induction of the luciferase activity compared with cells transfected with pcDNA3. Data shown are representative of two or three independent experiments with similar results. The significance of the differences was evaluated by Student's *t*-test (***$P<0.001$; **$P<0.01$; *$P<0.05$). (**d**, **e**) The expression of $p21^{Waf1}$ is upregulated by overexpression of myc-topors in small cell lung cancer cell SBC3 (**d**) and U2-OS cells (**e**). The expression of human $p21^{Waf1}$ was determined by quantitative real-time RT–PCR analysis as described in Materials and methods. Relative expression levels of $p21^{Waf1}$ were normalized to the levels of *β-actin* mRNA. The data shown are representative of two independent experiments with similar results. The significance of the differences was evaluated by Student's *t*-test (*$P<0.05$)

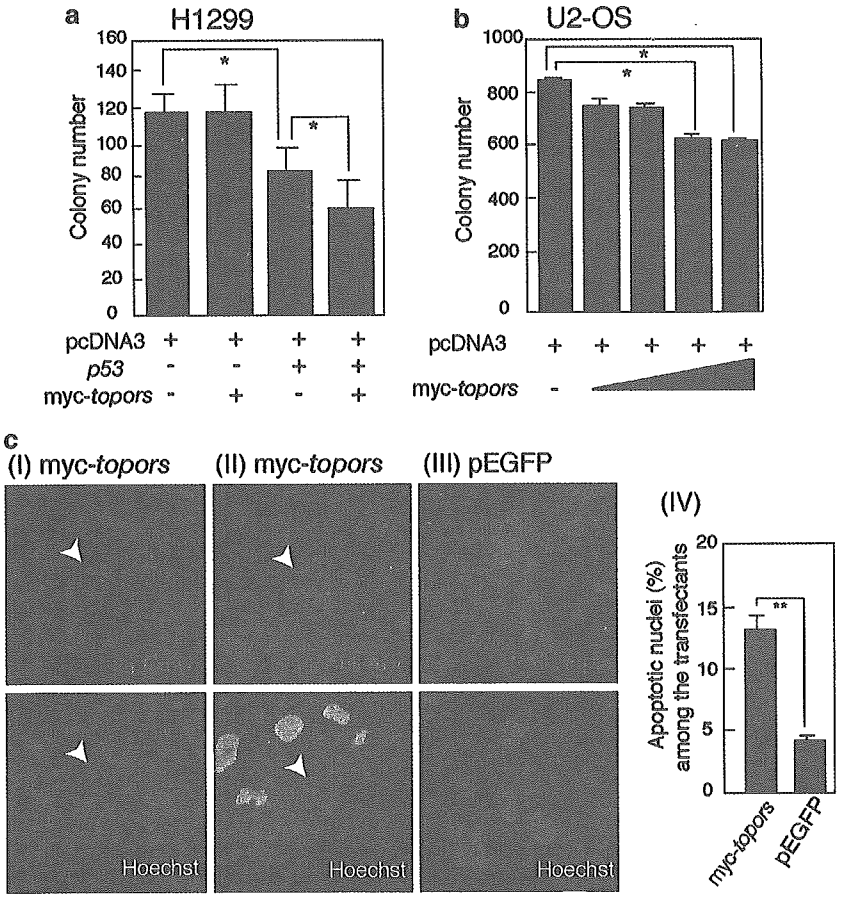

Figure 3 Enhancement of p53-dependent growth suppression and induction of apoptosis by the overexpression of topors. (**a**) The reduction in colony number by the transient overexpression of p53 is significantly enhanced by myc-topors in p53-deficient H1299 cells. (**b**) Increasing amounts of transfected myc-topors correlate with the reduction in colony number of U2-OS cells containing wild-type p53. Bars show the average numbers of colonies in triplicate experiments. The data shown are representative of three independent experiments with similar results. The significance of differences was evaluated by Student's *t*-test ($*P<0.05$). (**c**) Overexpression of myc-topors in U2-OS cells results in an increase in the number of apoptotic cells. U2-OS cells were transfected with either pcDNA3-myc-*topors* or pEGFP and transfected cells were identified by immunofluorescence staining with anti-myc monoclonal antibody or GFP expression, respectively (upper panels). Nuclear morphology was analysed after counterstaining with 1 μM Hoechst (lower panels). Cells overexpressing myc-topors frequently exhibit condensation (I) or fragmentation (II) of the nuclei, while GFP expression shows normal morphology (III). The percentages of apoptotic cells among >200 myc-topors- or GFP-positive cells were determined (IV). Values represent the means of three independent experiments. The significance of the differences was evaluated by Student's *t*-test ($**P<0.01$)

compared with the parental U2-OS cells and U2-OS cells transfected with empty vector (V-1) (Figure 4c). Of note, *topors* sta-1 cells grew more slowly than *topors* sta-2 cells, suggesting that the growth rate correlated inversely with the level of myc-topors expression in the respective cell lines. Next, asynchronous cultures of these transfectants and the parental cells were collected at 48 h after culture and their cell cycle distribution was analysed by flow cytometry. As shown in Figure 4d (cisplatin (−)) and e, *topors* sta-1 and *topors* sta-2 cells displayed a significant increase in the percentage of cells in G1 phase as compared with U2-OS and V-1 cells. A slight but reproducible increase in the sub-G1 fraction was seen exclusively in *topors* sta-1 cells (even without cisplatin treatment; see below), suggesting the constitutive occurrence of apoptosis in the *topors* sta-1 transfectants (Figure 4d and f (cisplatin (−))). The severe growth retardation of U2-OS cells stably expressing myc-topors might therefore result from both a prolonged G1 phase and a subtle induction of apoptosis. Comparison of the *topors* sta-1 and *topors* sta-2 results suggests that overexpression of topors can result in growth arrest and/or apoptosis depending on the degree of topors expression and the particular cellular context.

Stabilization of p53 by overexpression of topors

To determine whether the growth retardation produced by the stable overexpression of myc-topors was linked to the activation of p53, we next examined the expression of p53 and its response gene product, $p21^{Waf1}$ (Harper *et al.*, 1993), in permanent transfectants. p53 was more abundantly expressed in both *topors* sta-1 and *topors* sta-2 stable transfectants than in control cell lines and the expression of $p21^{Waf1}$ was greater in both topors

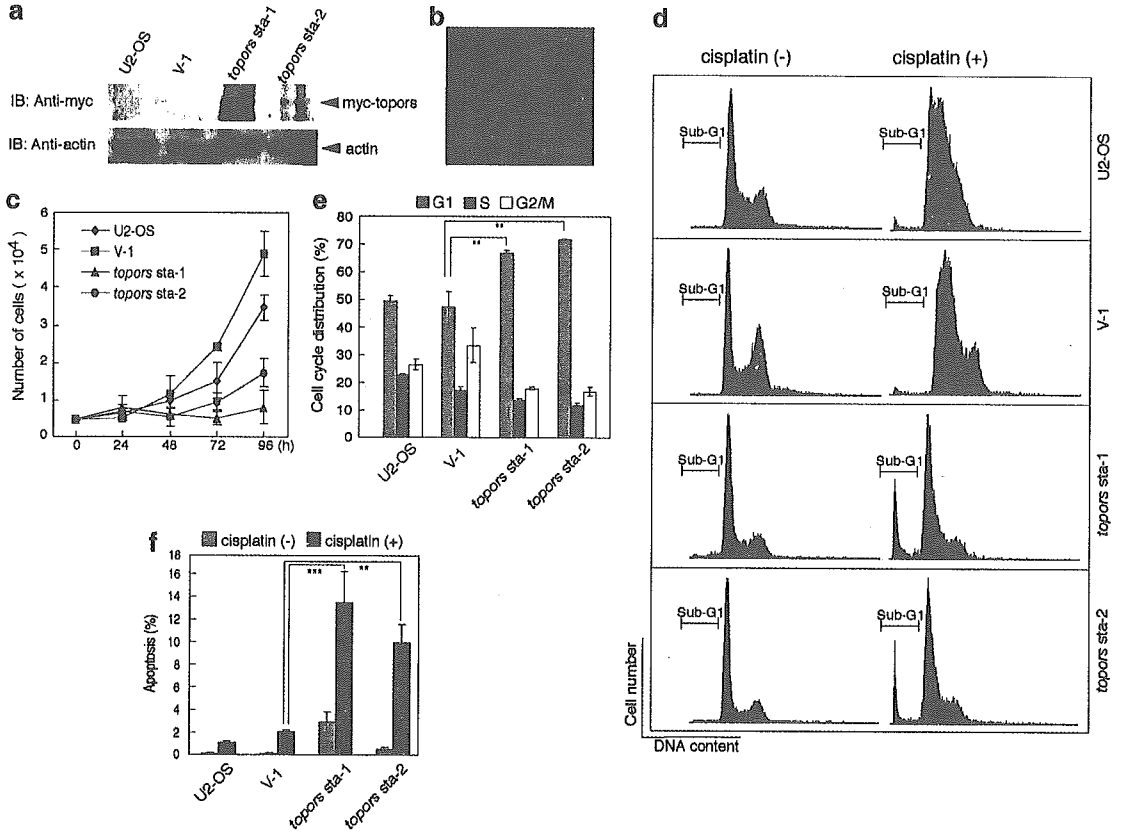

Figure 4 Cell cycle arrest and DNA damage-mediated apoptosis in U2-OS cells stably overexpressing myc-topors. (**a**) The expression of myc-topors in parental U2-OS cells and stable empty pcDNA3 vector (V-1) and pcDNA3-myc-*topors* (*topors* sta-1 and sta-2) transfectants as revealed by immunoblotting analysis using a polyclonal anti-myc antibody. The expression of actin is shown below as a loading control. (**b**) The expression pattern of myc-topors in *topors* sta-1 cell nuclei as revealed by immunofluorescent staining with anti-myc monoclonal antibody. (**c**) Growth rates of the indicated cells. The indicated cells were seeded at a density of 0.5×10^4 cells/well (12-well plate) and cell numbers were determined 1, 2, 3 and 4 days later. Average cell numbers at each time point determined in triplicate experiments are shown; standard deviations are shown in parentheses. Representative results of three independent experiments are shown. (**d**) Exponentially growing stable transfectants and control cells treated without or with cisplatin were stained with propidium iodide (PI) and subjected to FACS analysis. Representative FACS profiles of each cell line without (left) or with (right) cisplatin treatment are shown. Sub-G1 fractions are indicated. (**e**) Cell cycle profiles of exponentially growing U2-OS-derived cells as revealed by FACS analysis are shown by histograms. (**f**) Frequency of apoptotic cells among cells treated without (−) and with (+) cisplatin is shown by histograms. Values are the average percentages from triplicate experiments, and standard deviations are shown in parentheses. The experiments were repeated three times with essentially similar results. The significance of differences was evaluated by Student's *t*-test (***$P<0.001$; **$P<0.01$)

stable transfectants than in controls (Figure 5a). The increased level of $p21^{Waf1}$ protein correlated with the topors-enhanced expression of *p21*^{Waf1} mRNA in small cell lung cancer cells and U2-OS cells shown above (Figure 2d and e). Importantly, the upregulation of p53 and $p21^{Waf1}$ proteins in *topors* sta-1 was stronger than in *topors* sta-2, consistent with the relative expression level of ectopic myc-topors and the severity of the growth phenotypes in the two cell lines. The levels of expression of the p53 protein could also be increased by transient overexpression of myc-topors in U2-OS cells and p53-deficient large cell lung carcinoma H1299 cells, which were cotransfected with both FLAG-tagged *p53* and myc-*topors* (Figure 5c and d). Since the level of *p53* transcript was not significantly different in either of the permanent transfectants compared to controls (Figure 5b), it is likely that the increase in the amount of p53 protein was due to its stabilization. To investigate whether an increased protein half-life contributed to the elevated levels of p53 observed, we then determined the decay rate of p53 protein without and with topors overexpression. At 24 h after culture of the empty vector stable cells (V-1) and *topors* sta-2 cells, or 24 h post-transient transfection of p53-deficient human large cell lung carcinoma H1299 cells with FLAG-*p53* along with either pcDNA3 or pcDNA3-myc-*topors*, cells were treated with the protein synthesis inhibitor cycloheximide at a final concentration of 100 μg/ml for 0, 2, 4 and 6 h. The expression of p53 was then examined by immunoblotting for each time point and normalized by reference to the level of actin in each sample. As shown in Figure 5e, the p53 protein possessed a greater half-life in *topors* sta-2 cells compared with V-1 vector-transfected U2-OS cells. Similarly, the half-life of p53 was prolonged in the presence of topors compared to that of p53 cotransfected with pcDNA3 vector in p53-deficient

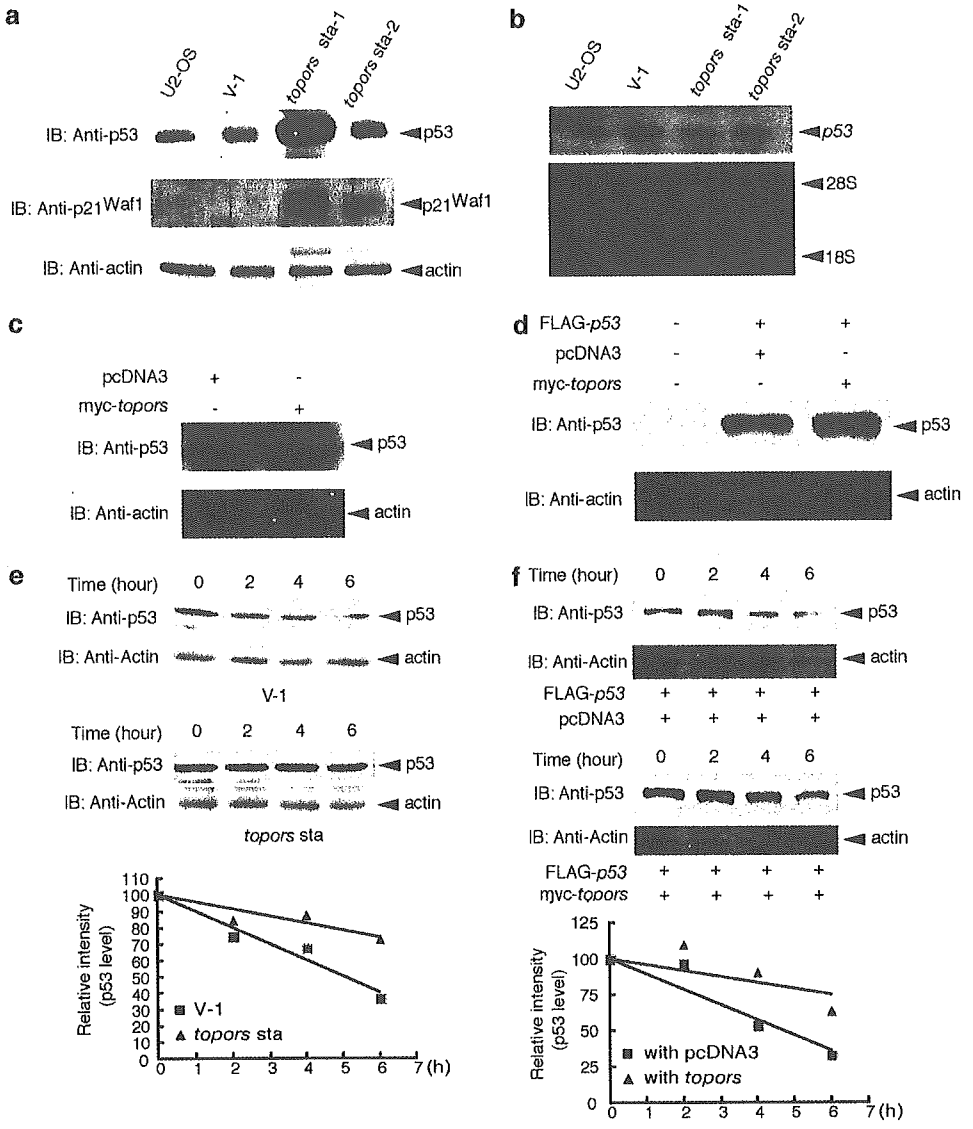

Figure 5 Stabilization of p53 protein by overexpression of myc-topors. (**a**) The expressions of p53 and $p21^{Waf1}$ in parental U2-OS cells and stable transfectants of pcDNA3 vector (V-1) and pcDNA3-myc-*topors* (*topors* sta-1 and sta-2) as revealed by immunoblotting analysis. The expression of actin is shown as a loading control. (**b**) The expression of *p53* transcript in each cell line as revealed by RNA blot analysis (upper panel). Ethidium bromide staining of 28S and 18S ribosomal RNA is shown as a loading control (lower panel). (**c**) The expression of p53 in U2-OS cells after transfection with pcDNA3 or pcDNA3-myc-*topors*. The expression of actin is shown as a loading control. (**d**) The expression of p53 in H1299 cells after transfection without or with FLAG-*p53* in the presence of pcDNA3 or pcDNA3-myc-*topors*. The expression of actin is shown as a loading control. (**e**, **f**) Increase in the half-life of p53 by topors. At 24 h after culture of pcDNA3 stable cells (V-1) and *topors* sta-2 cells (**e**), or at 24 h after transient transfection of p53-deficient H1299 cells (**f**) with expression plasmid of FLAG-*p53* along with pcDNA3 or pcDNA3-myc-*topors*, cycloheximide was added to the culture medium and the cells were extracted at the indicated time points. Whole-cell lysates were subjected to immunoblotting. The relative intensities of p53 were quantified by densitometric scanning, which normalized to actin, and are represented graphically

H1299 cells (Figure 5f). Taken together, these data suggest that expression of topors increases p53 levels by stabilizing p53 protein and thereby enhancing its ability to limit cell growth.

topors expression is induced by DNA damage

Our finding that transient or stable transfection of topors upregulates p53 levels suggests that topors could be a rate-limiting factor in the regulation of p53 function. If this is the case, a quantitative alteration of topors expression in a given cell could affect its apoptotic response to genotoxic reagents. To address this possibility, exponentially growing U2-OS cells or stable transfectants were treated with 20 μM cisplatin for 24 h, and the cells were then subjected to the cell cycle analysis. Following cisplatin treatment, both *topors* sta-1 and *topors* sta-2 cells demonstrated significantly increased sub-G1 fractions compared to the control cells (Figure 4d and f). The fraction of apoptotic cells among the *topors* sta-1 and *topors* sta-2 transfectants reached 80–90% after 48 h of cisplatin